2015•2016

FACULTEIT GENEESKUNDE EN LEVENSWETENSCHAPPEN

master in de biomedische wetenschappen

Masterproef

Targeting the pro-inflammatory and cytotoxic environment to improve functional recovery after SCI

Promotor :
Prof. dr. Sven HENDRIX

Copromotor :
dr. Nathalie GEURTS

Joren Jonckers

Scriptie ingediend tot het behalen van de graad van master in de biomedische wetenschappen

De transnationale Universiteit Limburg is een uniek samenwerkingsverband van twee universiteiten in twee landen: de Universiteit Hasselt en Maastricht University.

universiteit hasselt

KNOWLEDGE IN ACTION

Universiteit Hasselt | Campus Hasselt | Martelarenlaan 42 | BE-3500 Hasselt
Universiteit Hasselt | Campus Diepenbeek | Agoralaan Gebouw D | BE-3590 Diepenbeek

universiteit hasselt | Maastricht University

2015•2016
FACULTEIT GENEESKUNDE EN LEVENSWETENSCHAPPEN
master in de biomedische wetenschappen

Masterproef

Targeting the pro-inflammatory and cytotoxic environment to improve functional recovery after SCI

Promotor :
Prof. dr. Sven HENDRIX

Copromotor :
dr. Nathalie GEURTS

Joren Jonckers
Scriptie ingediend tot het behalen van de graad van master in de biomedische wetenschappen

universiteit hasselt | Maastricht University

Table of contents

Acknowledgements

During the last eight months, I was able to perform my senior practical training at the Morphology department of the Biomedical research institute (BIOMED). Without the support of several people, the senior internship and the writing of this thesis would not have been possible. Therefore, I would like to thank everyone who helped me during this exciting period.

First of all, I would like to thank my promotor Prof. dr. Sven Hendrix for the opportunity to perform my senior practical training in his research group. Thank you for your guidance, critical view and expertise that have helped me to become the skilled and critical researcher that I am today.

A big thank you goes out to my co-promotor dr. Nathalie Geurts and my daily supervisor drs. Stefanie Lemmens. Since my arrival at BIOMED, you made me feel part of your great team. Moreover, I am grateful for the trust and responsibility that I received from you both since the beginning. This allowed me to grow as an independent scientist. Nathalie, thank you for valuable criticism and kindness, you were always there to help me when I needed it. Stefanie, thank you for being there every single day for me. I am grateful for your guidance, support and for the practical things you have learned me. Becoming a skilled researcher would not have been possible without your help. Furthermore, a word of appreciation goes out to all the other members of the morphology group, who were always ready to answer my questions.

I also want to thank my second examiner dr. Myriam Gou Fabregas for sharing her extensive research knowledge with me. Thank you for all your help, especially with the production of lentiviral vectors.

Lastly but certainly not least, I would like to thank my parents, sister and classmates who helped me during difficult periods, not only this year, but throughout my whole education.

Joren Jonckers

June 8, 2016

List of abbreviations

3-MA	3-methyladenine
Abcg5$^{-/-}$	ATP-binding cassette sub-family G member knock out
AIF	Apoptosis-inducing factor
Apaf-1	Apoptotic protease activating factor -1
Arg-1	Arginase-1
Arg-1 BMDMs	Arg-1-overexpressing BMDMS
Atg5	Autophagy protein 5
BBB	Blood brain barrier
Bid	BH3 interacting-domain death agonist
BMCs	Bone marrow cells
BMDMs	Bone marrow-derived macrophages
BMS	Basso Mouse Scale
catD	Cathepsin D
CNS	Central nervous system
CSPG	Chondroitin sulphate proteoglycan
CST	Corticospinal tract
DNA	Deoxyribonucleic acid
ECM	Extracellular matrix
ER	Endoplasmic reticulum
FBS	Fetal bovine serum
HDL	High density lipoproteins
HEK	Human embryonic kidney
iFCS	Heat inactivated fetal calf serum
IFN- y	Interferon- y
IL	interleukin
IL-13 BMDMs	IL-13-overexpressing BMDMs
IL-13R	IL-13 receptor
iNOS	Inducible nitric oxide synthase
LC3-II	LC3-phosphatidulethanolamine conjugate
LCM	L929's conditioned medium
LPS	Lipopolysaccharide
LV	Lentiviral vector
MSCs	Mesenchymal stem cells
NO	Nitric oxide
PBS	Phosphate buffered saline
Pep-A	Pepstatin-A
PFA	Paraformaldehyde
PS	Plant sterols
qPCR	Quantitative polymerase chain reaction
rIL-13	Recombinant IL-13
ROS	Reactive oxygen species
RT	Room temperature
SCI	Spinal cord injury
TBS-T	Tris buffered saline 0.05% Tween- 20
TGF-β	Transforming growth factor- β
Th	T helper
TNF-α	Tumor necrosis factor-α
WT	Wildtype

Summary

Most neurological disorders associated with spinal cord injury (SCI) are severe and permanent since the central nervous system (CNS) has a limited intrinsic ability to regenerate. This failure of regeneration is also partly due to inflammatory and neurotoxic processes that take place at the SCI lesion site and thereby create a growth-inhibitory microenvironment. Increasing evidence indicates that modulation of this hostile microenvironment can result in an improved functional recovery after SCI. However, most treatment strategies lack the feasibility to be translated into clinical applications. Therefore, the search for new and improved SCI treatment strategies is ongoing.

During the first subproject, we evaluated the potential of IL-13 overexpressing BMDMs (IL-13 BMDMS) to diminish the abundant M1 macrophage population present at the SCI lesion site. It is hypothesized that IL-13 BMDMs obtain an M2 phenotype and create an IL-13-enriched environment which skews other macrophages towards an M2 phenotype, resulting in a more permissive environment for spinal cord regeneration. Our results indicate that IL-13 BMDMs secrete significantly increased levels of IL-13 compared to control conditions. Moreover we show that IL-13 BMDMs are able to create an IL-13-enriched environment, polarizing themselves and other naïve macrophages towards an M2 phenotype *in vitro.* Further *in vivo* studies have to reveal the potential of IL-13 BMDMs to improve the functional recovery after SCI.

In a second subproject, the goal was to counteract the global pro-inflammatory response which is responsible for the growth-inhibitory environment. Since articles highlight the anti-inflammatory effects of plant sterols (PS), we hypothesize that PS improve the functional recovery after SCI by suppressing neuro-inflammation. However, our *in vivo* experiments indicate that PS alone are not sufficient enough to improve the functional recovery after SCI.

Besides this inflammatory response, also neurotoxic pathways contribute to the growth-inhibitory microenvironment at the lesion site. After SCI, different apoptotic inducers permeabilize lysosomes in neurons, astrocytes and immune cells. One of the neurotoxic compounds leaking out of the disrupted lysosomes is cathepsin D (catD). Therefore, in a third subproject, we hypothesized that blocking catD would improve the functional recovery after SCI. Nevertheless, our data indicate that the catD inhibitors pep-A and 3-MA did not affect the functional recovery in SCI mice.

Taken together, we can conclude that PS and catD inhibitors are not sufficient enough to improve the functional recovery after SCI. Therefore, further research should focus on IL-13 BMDMs which are already shown *in vitro* to polarize macrophages towards an M2 phenotype.

Samenvatting

De meest voorkomende neurologische aandoeningen, geassocieerd met ruggenmergletsels zijn permanent omdat het centrale zenuwstelsel slechts een gelimiteerde capaciteit bezit voor zelfregeneratie. De ontstekings- en neurotoxische processen die ontstaan na ruggenmergschade spelen een belangrijke rol in het verdere verloop van de aandoening omdat ze een schadelijke omgeving creëren die het herstel van zenuwbanen tegenwerkt. Onderzoek toont aan dat het moduleren van deze groei-inhiberende omgeving gepaard gaat met een verbeterd functioneel herstel. Omdat de huidige behandelingsstrategieën vaak niet vertaald kunnen worden in klinische applicaties, is de zoektocht naar verbeterde therapieën nog steeds lopende.

In een eerste deelproject werd het anti-inflammatoire potentieel van macrofagen, die IL-13 tot overexpressie brengen (IL-13 macrofagen), onderzocht. Onze hypothese luidt dat IL-13 macrofagen zichzelf, alsook andere macrofagen, kunnen polariseren naar een M2 fenotype door het produceren van functioneel IL-13. Onze resultaten tonen aan dat IL-13 macrofagen significant meer IL-13 uitscheiden in vergelijking met de controle condities. Ze voorzien de omgeving dus van een hoge concentratie aan IL-13, waardoor ze naïve macrofagen *in vitro* kunnen polariseren naar een M2 fenotype. Toekomstige *in vivo* studies zullen uitwijzen of IL-13 macrofagen het functioneel herstel na ruggenmergschade kunnen bevorderen. Een tweede deelproject had tot doel de globale pro-inflammatoire omgeving te moduleren. Omdat plant sterolen (PS) omschreven worden als anti-inflammatoir in de literatuur, stellen wij de hypothese dat PS het functionele herstel na ruggenmergschade kunnen bevorderen. Onze hypothese werd echter niet bevestigd, sinds PS geen effect vertoonden op het functionele herstel.

Ook neurotoxische mechanismes dragen bij tot de groei-inhiberende omgeving. Na ruggenmergschade komen er verschillende biologische stoffen vrij die lysosomen van endogene cellen permeabiliseren. Een van de neurotoxische stoffen die uit de geperforeerde lysosomen vrijkomt is cathepsine D (catD). In een derde deelproject is de hypothese dat het blokkeren van catD resulteert in een verbeterd functioneel herstel. Desondanks toonden onze data aan dat de catD inhibitoren pep-A en 3-MA niet voor een verbeterd functioneel herstel konden zorgen.

In deze studie tonen we aan dat zowel PS als catD inhibitoren onvoldoende zijn om ruggenmergschade te herstellen. Aangezien *in vitro* al aangetoond is dat IL-13 macrofagen in staat zijn om naïve macrofagen te differentiëren naar een M2 fenotype, zal toekomstig onderzoek zich focussen op het effect van deze IL-13 macrofagen *in vivo*.

1. Introduction

1.1. Traumatic spinal cord injury

Spinal cord injury (SCI) is a disabling condition which causes damage to the central nervous system (CNS), leading to the loss of both ascending and descending axonal tracts and demyelination. Due to the limited intrinsic ability of the CNS to regenerate, neurological disorders associated with SCI are mostly severe and permanent, resulting in motor deficits and even paralysis (1). Besides the loss of sensory and motor capabilities, many other problems are associated with SCI such as bladder infections and respiratory difficulties. Since SCI often results in lifelong disabilities, it aggravates the patients' quality of life considerably. In addition to the physiological and physical trauma, there is a substantial financial burden for the patients, family and even the society (2, 3).

Worldwide, the number of patients living with an SCI is estimated on 2.5 million people, with more then 130 000 new cases reported each year (4). The majority of these injuries are caused by vehicle crashes, sports accidents, falls and violence. Despite the aggravated health condition after SCI, only one drug, i.e. methylprednisolone, has been approved as a therapy. However, data revealed that this drug only has limited effectiveness. Therefore, renewed insights into the pathology of SCI are essential to boost the development of novel and effective treatment strategies. The complicated pathophysiology following SCI is, however, a major bottleneck in therapy design (5). The primary mechanical injury results in extensive neuronal cell death and transected axons **(Figure 1A)**. This initial lesion is extended by multi-faceted secondary degenerative cascades that further aggravate the clinical outcome. One of these major cascades is the initiation of an inflammatory response, leading to the infiltration of immune cells into the lesion area. Key players in this inflammatory reaction are microglia/macrophages, astrocytes and T-cells **(Figure 1B)**. Other underlying mechanisms include the formation of free radicals, inflammation-mediated cell death, demyelination of surviving axons, glutamatergic excitotoxicity and ischemia (5, 6). These processes evoke additional tissue damage and more importantly, they will limit the functional recovery after SCI (3). In this context, a dense glial scar formed by astrocytes will surround the central cavitation **(Figure 1C)**. In the acute phase after injury, scarring is regarded as advantageous since it limits the secondary damage and is crucial for regaining tissue integrity. However, in a later stadium it will literally block axons to regenerate, both physically and chemically (7). This is because the glial environment is rich in axonal growth-inhibitory molecules like chondroitin sulphate proteoglycans (CSPGs), which are released by hypertrophic astrocytes. Other inhibitors that form a hurdle for axon regeneration are associated with specific myelin and extracellular matrix (ECM) compounds such as laminin and fibronectin (extrinsic adult CNS barriers) (8).

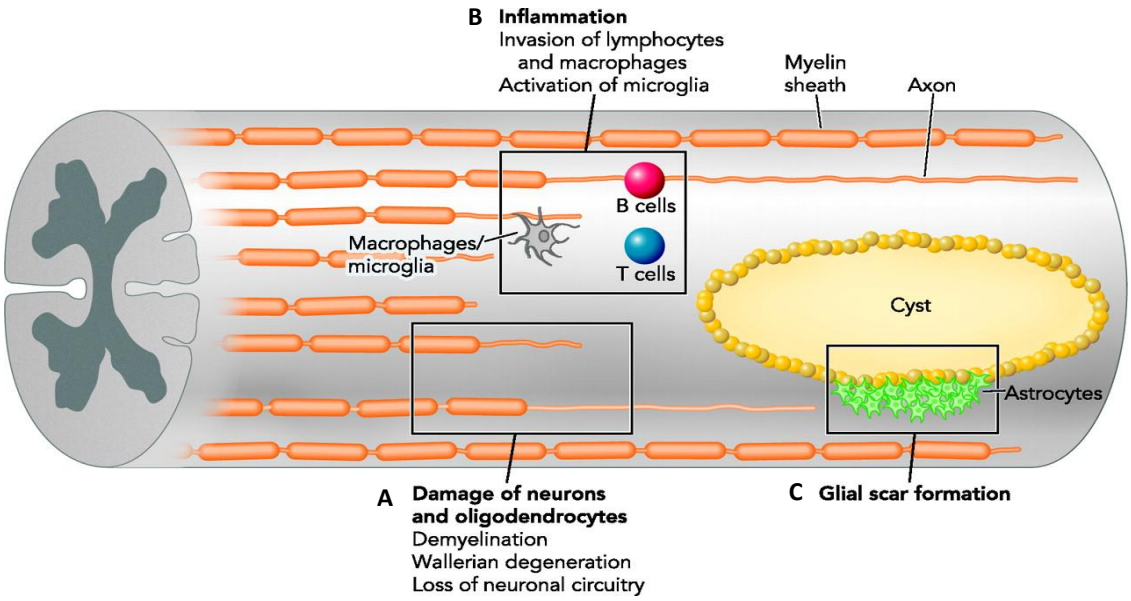

Figure 1: Pathophysiology of spinal cord injury. The processes associated with SCI include a primary mechanical injury as well as a secondary injury initiated by an inflammatory response. A) The primary mechanical insult results in neuronal- and oligodendrocyte cell death and damaged axons. B) After the initial mechanical insult, secondary injury cascades further aggravate the cellular damage. This is characterised by an inflammatory response, leading to the infiltration and activation of immune cells. C) Later on, a glial scar is formed with reactive astrocytes as major components. *SCI, spinal cord injury*. Figure adapted from Obermair *et al*, Physiology, 2008.

1.2. Post-traumatic inflammation following SCI

Besides the initial mechanical injury, SCI evokes an inflammatory response inside the lesion, which aggravates the injury by causing additional tissue damage and neurodegeneration (9). Macrophages derived from both infiltrating monocytes and tissue resident microglia accumulate rapidly after SCI within the epicenter of the lesion. Hence, the role of these macrophages during SCI pathology has become an interesting research topic (10, 11).

Macrophages display a broad plasticity and can adapt their phenotype and functions depending on which type of stimuli they are exposed to. Consequently, the local microenvironment after SCI consists of different macrophage populations. Depending on the activation status and phenotype, macrophages may not only initiate the secondary injury cascades, but they also contribute to tissue repair. The two primary macrophage subsets are the classically activated M1 and alternatively activated M2 macrophages, which are considered as pro-inflammatory and anti-inflammatory, respectively (12). Although this macrophage phenotype classification is broadly implemented, the dichotomy of M1/M2 might be too simplistic because many intermediate macrophage phenotypes exist. Depending on the stimulus, the factors they secrete and the markers they express, M2 macrophages are classified as M2a, M2b and M2c macrophages amongst others. (11). Still, despite this linear classification has some limitations, this concept provides a useful framework to further define the role of macrophages during post-traumatic SCI.

Lipopolysaccharide (LPS) and T helper type 1 (Th1) cell-derived cytokines such as interferon-γ (IFN-γ) and tumor necrosis factor-α (TNF-α) promote macrophage differentiation towards an M1 phenotype. These cells secrete high levels of pro-inflammatory cytokines such as IFN-γ, TNF-α, interleukin (IL)-6, IL-23 and other toxic mediators such as reactive oxygen species (ROS) (e.g. nitric oxide (NO) and superoxide). These are crucial for host defense but also cause toxic damage to vital tissue. Moreover, these cells contribute to axonal retraction and the formation of a growth-inhibitory glial scar. This creates a hostile environment at the lesion site, thereby suppressing the ability of axons to regenerate (11). Contrarily, T helper type 2 (Th2) cell-derived cytokines polarize macrophages towards the alternative M2 phenotype. These cells balance the pro-inflammatory microenvironment formed by M1 macrophages by producing anti-inflammatory cytokines such as transforming growth factor-β (TGF-β), IL-10, IL-13 and IL-4. Furthermore, they produce growth factors, promote angiogenesis, provide neuro/axonal trophic support and degrade the inhibitory glial scar components, resulting in the stimulation of axon regeneration. Therefore, these M2 macrophages are able to reduce the harmful microenvironment associated with the secondary injury process of SCI (9, 11).

Although both M1 and M2 macrophages coexist during the first week at the SCI lesion site, only M1 macrophages persist at the lesion epicenter until day 28. Recently, Kigerl *et al.* showed a rapid and prolonged M1 macrophage onset after SCI, which overwhelms the limited and transitory M2 macrophage response. Since M1 macrophages are neurotoxic and M2 macrophages rather induce axonal regeneration, this high M1:M2 ratio evokes major detrimental implications for the CNS repair after SCI (13). Therefore, reducing the M1 while increasing the M2 macrophage population during SCI might be an interesting new treatment approach to improve neuroregeneration **(Figure 2)**.

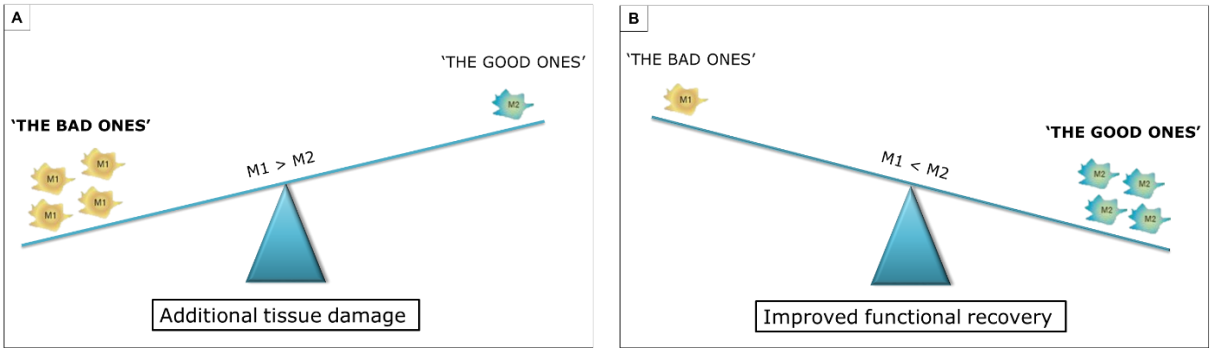

Figure 2: Post-traumatic inflammation after SCI. A) During SCI, there is a high M1:M2 macrophage ratio, leading to additional tissue damage due to the neurotoxic effects of M1 macrophages. Therefore, these M1 macrophages are also considered as 'the bad ones'. B) Modulating the inflammatory response by skewing the M1 macrophages towards an M2 phenotype can result in a more effective neuroregeneration. This is because M2 macrophages can improve axonal regeneration. Therefore, these macrophages are also considered as 'the good ones'. *SCI, spinal cord injury.*

1.3. Adoptive transfer of IL-13-overexpressing BMDMs to improve the functional regeneration after SCI

The Th2-immune response is a crucial reaction of the immune system against allergic reactions and invading helminths (14). A key mediator in this immune response is the cytokine IL-13, which is mainly secreted by Th2-cells but also by macrophages and microglial cells, amongst others. It exerts its biological effects via interaction with a specific cell surface receptor, expressed on many immune cells, including B lymphocytes, macrophages, and mast cells (15). Two subtypes of the IL-13 receptor (IL-13R) exist: the type I receptor is a heterodimer of IL-4Rα and IL-13Rα1 which can also bind to IL-4, while the type II receptor consists of an IL-13Rα2 chain and binds exclusively to IL-13.

IL-13 is able to suppress the production of pro-inflammatory cytokines such as TNF-α, IFN-γ and IL-6 from activated microglial cells (16, 17). Moreover, it polarizes macrophages and microglia towards an anti-inflammatory M2 phenotype (18). These events underscore the potency of IL-13 as a therapeutic agent in the field of different CNS pathologies characterized by an intense neuro-inflammatory phase, such as SCI. As described previously, M1 macrophages are the 'bad ones' by being neurotoxic and growth-inhibitory, while M2 macrophages are the 'good ones' by stimulating neuroprotection and regeneration of nerve tissue. Therefore, decreasing the M1 and increasing the M2 macrophage population at the SCI lesion site can protect neurons, maintain residual myelin, initiate tissue repair and eventually improve normal locomotor functioning (12, 13, 19, 20).

IL-13 is a well-suited candidate to directly polarize the M1 macrophages towards M2. Moreover, it can create a positive feedback loop that further enriches the M2 macrophage population, as Il-13 downregulates Th1-cell differentiation while upregulating Th2-cell activation (12, 13). These T-cells will express anti-inflammatory mediators which may prevent M2 macrophages from shifting back towards M1 (21). Besides its anti-inflammatory capacity, IL-13 harbors pro-regenerative competences. Unpublished data from our research group indicate that IL-13 acts neuroprotective and stimulates neurite outgrowth from primary neurons and organotypic brain slices.

Hence, modulating the lesion site into an IL-13-enriched microenvironment may represent a promising strategy for tissue repair after SCI. Preliminary data from our group already revealed that mice treated with IL-13-overexpressing mesenchymal stem cells (MSCs) show a significantly improved functional recovery after SCI (22). However, by using IL-13-overexpressing macrophages instead of MSCs, the M2 macrophage population can be further amplified at the lesion site. Moreover, it is possible that macrophages have an increased intrinsic ability to migrate towards the lesion site.

In the present study, bone marrow-derived macrophages (BMDMs) are transduced with an IL-13 lentiviral vector (LV), in order to make them overexpress IL-13. These IL-13 BMDMs are phenotyped and their ability to secrete therapeutic levels of IL-13 is investigated. Eventually, in a second part of the study, IL-13-overexpressing BMDMs (further renamed as IL-13 BMDMs) will be administered to SCI mice. The goal of this study is to elucidate whether the IL-13 BMDMs adopt an M2 phenotype and thereby create an anti-inflammatory environment prone to axon regeneration. Furthermore, this project may unravel the molecular mechanisms by which IL-13 modulates macrophage function *in vitro* and *in vivo*. We hypothesize that IL-13 BMDMs will polarize towards an M2 phenotype and create an IL-13-enriched environment which skews endogenous macrophages towards an M2 phenotype resulting in an improved functional regeneration after SCI. Eventually, this study may provide new insights in the use of IL-13 BMDMs as a potential therapy for SCI patients.

1.4. Adoptive transfer of arginase-1-overexpressing BMDMs to improve the functional regeneration after SCI

The high M1:M2 ratio at the SCI lesion site leads to increased levels of inducible nitric oxide synthase (iNOS) because it is highly expressed in activated M1 macrophages (23). iNOS is known to produce NO as long as its substrate L-arginine is available (24). In physiological conditions, NO is regarded as a well-suited effector molecule used by immune cells against infiltrating micro-organisms. However, persistent high levels of iNOS during SCI can result in the production of toxic NO levels (25). Since NO is a free radical, high levels of NO can oxidize proteins, deoxyribonucleic acid (DNA) and cell membranes. Moreover, its toxic properties are increased when it reacts with a superoxide anion radical, to create the highly toxic molecule peroxynitrite, which has been shown to cause neuronal dysfunction and cell death in numerous degenerative diseases (24, 26). Arginase-1 (Arg-1) can suppress this NO production by competing with iNOS for the L-arginine substrate. As a result, it can decrease the NO production and thereby limit the toxic potential of NO. In addition, when Arg-1 hydrolyzes L-arginine to ornithine and urea, it results in the production of polyamines, which are known to enhance the capacity of axons to overcome growth-suppressing effects (27, 28). These results indicate that Arg-1 can modulate the severity and progression of neurodegenerative processes, not only by limiting toxic agents, but also by stimulating axonal regrowth. However, to date, not much is known about the specific role of Arg-1 in the CNS. Therefore, further *in vitro* and *in vivo* studies are needed to assess the exact functional role of Arg-1 during several CNS disorders, including SCI.

The aim of this research project is to produce an Arg-1 lentiviral vector that is able to effectively transduce BMDMs, resulting in Arg-1-overexpressing BMDMs. Over the last decades, Arg-1 became one of the most popular markers for M2 macrophages (27). Yet, it is not known if Arg-1 can polarize macrophages towards an M2 phenotype. In a second part of the study, these Arg-1-overexpressing BMDMs (further renamed as Arg-1 BMDMs) will be administered into the injured spinal cord of mice using the same protocol as with the IL-13 BMDMs. Eventually, this project may indicate if Arg-1 BMDMs are able to improve functional recovery after SCI. Secondly, we intend to gain some knowledge about the role of Arg-1 in macrophage polarization in the CNS. Based on the beneficial effects of Arg-1 on lowering the toxic NO production and stimulating axonal growth via polyamines, we hypothesize that the functional recovery after SCI will be improved after adoptive transfer of Arg-1 BMDMs.

1.5. Targeting cathepsin D to improve the functional recovery after SCI

Besides the inflammatory response of macrophages, also other processes play an important role during the SCI pathophysiology such as the neurotoxic cathepsin D (catD) cascade. In the spinal cord, catD is expressed in many cells such as neurons, astrocytes and macrophages/microglia (29). After synthesis in the endoplasmic reticulum, procathepsin D (52 kDa) is targeted to intracellular vesicular components (e.g. lysosomes). After entering the lysosomal acidic environment, procathepsin D is cleaved, resulting in an intermediate form of catD (48 kDa). Eventually, further proteolytic cleavage in the lysosomes results in an active mature form of catD (34 kDa). The physiological function of this enzyme includes enzymatic degradation of intracellular proteins, cleavage of growth factors and hormones, and regulating various cell death processes (30). Recently, a significant increased expression of catD has been observed in the injured spinal cord (29, 31). Since multiple studies have reported a neurotoxic role for both intra- and extracellular catD during different CNS disorders, upregulated catD levels may be associated with important neurotoxic pathways during SCI and thereby limiting locomotor recovery.

During SCI, a broad range of apoptotic inducers can trigger lysosomal permeabilization in neurons, astrocytes and immune cells. This lysosomal leakage, resulting in the substantial release of proteolytic enzymes (e.g. catD) into the cytosol, can initiate multiple apoptotic cascades (30). In general, catD permeabilizes mitochondria indirectly by cleaving BH3 interacting-domain death agonist (Bid). As a result, released cytochrome c forms a complex with apoptotic protease activating factor-1 (Apaf-1) which eventually activates caspase 3, leading to cell death (32).

Although catD is normally targeted to the intracellular vesicles, it occurs that catD is also present in the extracellular environment. In certain physiological conditions, catD evades the normal lysosomal packaging mechanisms and is secreted in the extracellular environment. In addition, a secretome analysis revealed that catD is actively secreted by macrophages/microglia during neuroinflammation, contributing to the extracellular catD concentration (33). Extracellular catD can induce neurotoxicity without being enzymatically active, which suggests that the underlying mechanisms of inducing cell death are different from those initiated by intracellular catD. It has been shown that extracellular catD-induced neurotoxicity is associated with increased levels of autophagosome markers (e.g. LC3-phosphatidylethanolamine conjugate (LC3-II) and autophagy protein 5 (Atg5)), which indicates an uncontrolled autophagosome accumulation (32). Normally, the content of autophagosomes is degraded by specific hydrolytic enzymes after fusing with lysosomes (autophagy flux). Therefore, it is possible that extracellular catD causes a defective autophagosome clearance, resulting in endoplasmic reticulum (ER) stress-induced apoptosis **(Figure 3)** (32, 34). The exact mechanism of how catD can disturb the autophagy flux is still unknown. Although it remains speculative, defective lysosomes may lay at the basis of this impaired autophagy flux (34).

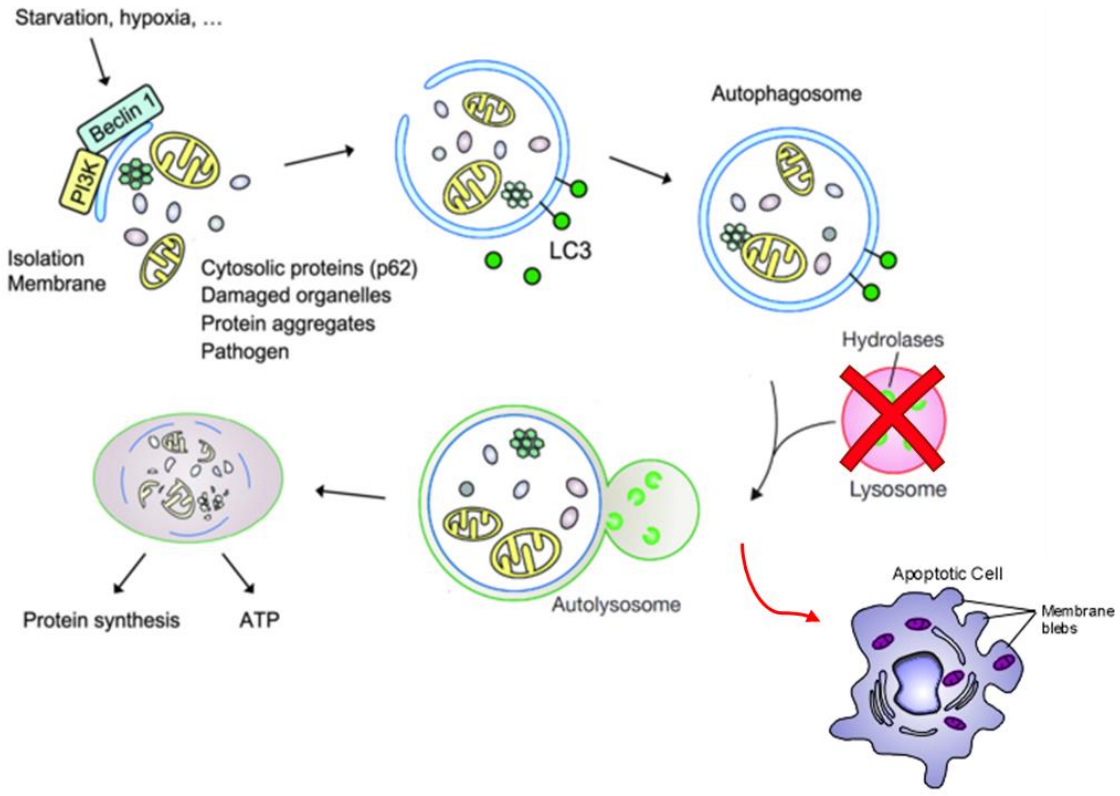

Figure 3: Impaired autophagy flux results in ER stress-induced apoptosis. Damaged organelles, protein aggregates and cytosolic proteins (p62) are sequestered by a double-membrane structure, the phagophore. This results in the formation of LC3-II-positive autophagosomes which will fuse with lysosomes to form autolysosomes. The sequestered content of the autophagosomes is degraded by the lysosomal hydrolases. Yet during SCI, defective lysosomes may impair this autophagic flux causing ER stress-induced apoptosis. *ER, endoplasmatic reticulum; LC3-II, LC3-phosphatidylethanolamine conjugate*. Figure adapted from Zhiping Xie *et al*, Nature, 2007.

Taken together, it becomes apparent that both intra- and extracellular catD can aggravate the post-traumatic SCI by inducing cell death by several mechanisms. Hence, inhibiting catD after SCI may represent a novel treatment strategy to limit the neurodegeneration accompanied with SCI. During this study, we investigated the time point where the catD concentration is maximal after inducing SCI. In a second part, the potential of catD inhibitors to improve the functional recovery after SCI is examined. Since catD can induce neurotoxicity in a broad variety of ways, we hypothesize that after SCI, the functional recovery is improved by inhibition of catD. Eventually, this project may provide new insights into the role of catD during the complex pathophysiology of SCI and the use of catD inhibitors to improve the locomotor recovery.

1.6. The effects of plant sterols on the regenerative processes after SCI

Plant sterols (PS) are naturally occurring compounds, which have gained substantial research interest. Since both humans and rodents are unable to produce PS, they are obligated to acquire them from their diet (nuts, fruits and vegetables). Interestingly, once in the systemic circulation, these dietary PS accumulate profoundly into the CNS (35). Vanmierlo *et al.* indicated that HDL-mediated transport of PS across the blood-brain barrier (BBB) is a key mechanism leading to an effective influx of PS into the CNS. Unlike cholesterol, PS are not able to be converted to their 24(S)-hydroxyl form in the CNS. Hence, PS cannot migrate from the CNS back into the circulation. Yet in some pathological or physiological conditions when the BBB is disrupted, the balanced exchange of PS between the circulation and the CNS may be disturbed (36).

Besides lowering the plasma cholesterol levels, PS have well described anti-inflammatory properties. It has been shown that plant sterols can modulate neuroinflammation in animal models for Alzheimer's disease and multiple sclerosis by (i) altering the transcription profile of macrophages, resulting in a reduced pro-inflammatory activation status, (ii) lowering the secretion of the pro-inflammatory cytokines IL-12 and TNF-α by peripheral blood mononuclear cells, (iii) decreasing CNS demyelination mediated by inflammation in an experimental autoimmune encephalomyelitis animal model, (iv) downregulating the amount of infiltrating immune cells into the inflamed CNS by altering the migratory characteristics of immune cells or by inhibiting the adhesive and chemotactic properties of endothelial cells (35). Due to these anti-inflammatory properties, many studies are focusing on the therapeutic potential of PS during different CNS disorders and diseases.

In the present study, we aim to elucidate the effect of PS during the secondary injury phase of SCI. Since most articles highlight the beneficial neuroinflammatory modulative effects of PS, we hypothesize that PS improve the functional recovery after SCI by suppressing the neuro-inflammation. To validate this hypothesis, a T-cut hemisection is induced in ATP-binding cassette sub-family G member knockout mice ($Abcg5^{-/-}$) and the functional recovery is measured according to the Basso mouse scale. Abcg5 is an important transporter on enterocytes which transports PS back into the intestinal lumen. As a result, the PS plasma levels in $Abcg5^{-/-}$ mice are significantly increased. During a second *in vivo* experiment, the effect of a PS-enriched diet on the functional recovery after SCI is investigated.

2. Experimental aims

Does adoptive transfer of IL-13 BMDMs in SCI mice results in an improved functional recovery?

During this study, it is investigated whether BMDMs transduced with an IL-13 LV are able to secrete elevated levels of IL-13. Moreover, we investigated the potential of IL-13 BMDMs to create an IL-13-enriched environment, polarizing themselves and other naïve macrophages towards an M2 phenotype. Eventually, these IL-13 BMDMs will be administered to SCI mice, to examine their effects on the functional recovery after SCI.

Is the functional recovery in SCI mice improved after adoptive transfer of Arg-1 BMDMs ?

The goal for this thesis project is to produce an Arg-1 lentiviral vector that is able to transduce BMDMs, resulting in Arg-1-overexpressing BMDMs.

Does inhibition of catD improves the functional regeneration after SCI ?

During this study, the time point where the catD concentration is maximal after inducing SCI is investigated. Next, both extra- and intracellular catD inhibitors are investigated on their potential to improve the functional recovery after inducing SCI.

Can PS improve the locomotor recovery after SCI by modulating the inflammatory environment ?

In this project, it is investigated if mice, predisposed to accumulate PS in their body, have an improved functional recovery after inducing SCI.

3. Materials and methods

3.1. Isolation and differentiation of bone marrow-derived macrophages

BMDMs were obtained by isolating murine primary bone marrow cells (BMCs) from both the tibia and femur of 9-16 weeks old C57BL/6J mice (Janvier, France). BMCs were collected by flushing the bone marrow cavities with sterile ice-cold 1x phosphate buffered saline (PBS) buffer. Cells were cultured for 10 days in RPMI 1640 medium (Invitrogen, Merelbeke, Belgium) supplemented with 10% heat inactivated fetal calf serum (iFCS) (FBS Superior, Biochrom AG, Germany), 1% penicillin/streptomycin (5000 units/ml penicillin, 5000 µg/ml streptomycin, Invitrogen, Belgium) and 15-30% L929 conditioned medium (LCM) at 37°C and 5% CO_2. Culture medium was changed partially or completely every 3 days. Eventually, cells cultured in the above medium were defined as M0 macrophages. For M1 polarization, M0 macrophages underwent a 48h incubation with 200 ng/µl LPS (Sigma, Belgium). Cells undergoing an incubation with 33,3 ng/µl recombinant IL-13 (rIL-13) (Sigma, Belgium) for 48h were defined as M2 macrophages (37).

3.2. Genetic modification of BMDMs

3.2.1. Lentiviral vector production

The pIRES-mIL-13-puro LV (8,5 x 10^7 pg p24/ml) used during this study was kindly provided by Prof. dr. Peter Ponsaerts (Antwerp University, Laboratory of Experimental Hematology). The pFUSPA-mArg-1-puro plasmid was constructed by inserting Arg-1 cDNA from the pcDNA3, 1-mArg-1 plasmid (Addgene, Cambridge, UK) into the pFUSPA-puro plasmid (Asc-1 digestion), using standard subcloning techniques. This pFUSPA-puro plasmid was generously provided by dr. Myriam Gou Fabregas (Hasselt University, Department of Morphology). Blunt end ligation of the Arg-1 cDNA insert into the pFUSPA-puro plasmid was performed using the Rapid DNA ligation kit (Roche, Brussels, Belgium) according to the manufactures' instructions. All plasmids were propagated in *E.coli* and purified using the Qiaprep Spin Miniprep Kit (Qiagen, Netherlands) or Nucleobond Xtra midi EF kit (Macherey Nagel, Germany) following the manufacturer kit guidelines. Correct orientation of the Arg-1 cDNA insert was confirmed by sequencing analysis.

The pFUSPA-Arg-1-puro LV production was performed as described previously in Tiscornia *et al.* (38). Briefly, human embryonic kidney (HEK293T) cells were cultured using high glucose Dulbecco's Modified Eagle Medium (DMEM) + 10% fetal bovine serum (FBS) (20 ml final volume) in 12 x 15 dishes

pre-coated with poly (l-lysine). The plasmid mix contained 12 µg of the transfer vector pFUSPA-Arg-1-puro plasmid, 15 µg of the packaging plasmid (psPAX) and 8 µg of envelop plasmid (pMDG2), 0,25M $CaCL_2$ and 2x BBS solution. When 85-90% confluency was reached, the transfection mixture was added to each plate and cells were incubated overnight at 37°C and 3% CO_2. At day 6, pFUSPA-Arg-1-puro LV were harvested from HEK293T cells supernatant.

3.2.2. Lentiviral vector transduction of BMDMs

For the LV transduction of the BMDMs, cells were transduced with the pFUSPA-mArg-1-puro or pIRES-mIL-13-puro viral particles (VP). Briefly, wells of an 24-well plate were seeded with 0.5 ml/well of the cell suspension (1,5 x 10^5 cells) in their standard culture medium and 1-10 µl/well of the LV (1 µl VP correlated with a multiplicity of infection (MOI) of 4, 2 µl VP with a MOI of 7, 5 µl with a MOI of 18 and 10 µl VP with a MOI of 36). Cells transduced with the pFUSPA-mArg-1-puro LV were incubated with 700 µl VP. Next, cells were incubated overnight at 37°C and 5% CO_2. after which residual LV and non-adherent cells were removed by performing a complete medium change. Antibiotic selection was performed with puromycin (2 µg/ml, InvivoGen, France) to select the transduced cells. The transduced BMDMs will be further renamed as IL-13/Arg-1-overexpression BMDMs (IL-13/Arg-1 BMDMs).

3.3. Immunocytochemistry

BMDMs were seeded at 88 464 cells/cm^2 in standard culture medium on glass cover slips (12 mm, Menzel GmbH, Braunschweig, Germany). When reaching 70-80% confluency, cells were fixed at room temperature (RT) in 4% PFA. Next, BMDMs were blocked in protein block (Dako, Carpinteria, USA) for 30 min at 4°C. The cells were incubated for 2h at RT with the primary antibodies, namely rabbit monoclonal anti IL-13 receptor-α1 (1:250, Abcam, UK), rat monoclonal anti IL-13 receptor-α2 (1:250, Abcam, UK), diluted in 1x PBS containing 1% protein block and 0,05% triton X-100 (Boehringer, Mannheim, Germany). Afterwards, cells were washed and incubated for 30 min at RT in the dark with the secondary antibodies: Alexa 488-labeled goat anti-rabbit antibody (1:250, Thermo Fisher, Belgium), Alexa 568-labelad goat anti-rat antibody (1:250, Thermo Fisher, Belgium), diluted in 1x PBS containing 1% protein block and 0,05% triton X-100. The specificity of the secondary antibodies was evaluated by omitting the primary antibody. After washing the cells, cellular nuclei were counterstained with 4',6-diamidino-2-phenylindole (1:100, DAPI, Invitrogen), diluted in 1x PBS containing 1% protein block and 0,05% triton X-100. Afterwards, BMDMs were mounted with fluorescent mounting medium (Dako, Carpinteria, USA). Pictures were taken with a Nikon Eclipse 80i fluorescent microscope equipped with a Nikon DS-2MBWc digital camera.

3.4. Fluorescence activated cell sorting

Flow cytometric analysis was performed on IL-13 BMDMs (MOI 36) in order to determine the expression of classical M2 macrophage markers. Untreated BMDMs and rIL-13/LPS-stimulated BMDMs were used as controls. Antibodies against Arg-1 and CD206 were used **(Table 1)**. As negative controls, unlabeled cells and isotype controls for the respective primary antibodies were used **(Table 1)**. Cultured cells were pelleted and resuspended in 100 µl fix perm for cell permeabilization (BD biosciences, US, new jersey). After incubation (20 min 4°C), 202 500 cells/well were seeded in a 96-well FACS plate and washed twice with FACS buffer. The antibodies were added to the cell suspension for 45 minutes at RT. Subsequently, labeled cells were analyzed with the flow cytometer FACS Aria (BD, Franklin lakes, NJ) for 10 000 events. Measurements were analyzed with BD CellQuest Pro™ Software (BD).

Table 1 – overview of the used antibodies and isotype controls for FACS analysis.

Antibody	Working dilution	Isotype control	Company/catalog nr.
Primary antibodies			
APC anti-mouse CD206	1:25	Rat IgG2a APC isotype control	Biolegend, 141707
APC anti-mouse Arg-1	1:3	sheep IgG PE isotype control	R&D systems, IC5868A
FITC anti-mouse CD45	1:125		Miltenyi Biotech 130-098-087
PE anti-mouse CD11b	1:167		Miltenyi Biotech 130-097-956
Isotype controls			
sheep IgG PE isotype control	1:3		R&D systems IC016A
Rat IgG2a APC isotype control	1:25		Ebioscience 56-4031-80

3.5. Western blot analysis

Total protein concentrations of samples **(Table 2)** were measured using the Pierce™ BCA Protein Assay Kit (Thermo Scientific, Belgium). Untreated BMDMs and rIL-13/LPS-stimulated BMDMs were used as controls. Proteins (4-8 µg) were separated on a 12% sodium dodecyl sulfate polyacrylamide gel for 40-50 min at 200 V. The proteins were transferred onto a 100% methanol-activated polyvinylidene fluoride membrane (Milipore, Belgium) for 90 minutes at 350 mA. After blocking the membrane for 60 min in a 5% non-fat dry milk in 1x Tris buffered saline supplemented with 0.05% Tween 20 (TBS-T), the membrane was incubated overnight with the primary antibody at 4°C **(Table 3)**. After washing the

membrane in 1x TBS-T, it was incubated with the secondary antibody at RT for 60 min **(Table 3)**. β-actin was used as an internal control. Signal detection was performed using the Pierce™ ECL Western Blotting Substrate (Thermo Scientific). Images were taken with the ImageQuant LAS 4000 Mini and analyzed with ImageQuant TL software (GE Healthcare, Belgium).

Table 2 - List of samples used for western blot analysis

Samples	Host	Company
BMDMs stimulated with LPS, IFN-y, IL-4 and rIL-13	BALB/c mice	Janvier, France
BMDMs transduced with IL-13 LV (MOI of 36)	C57BL/6J mice	Janvier, France
BMDMs cultured with 100 µl of conditioned media from IL-13 BMDMs	C57BL/6J mice	Janvier, France
HEK293T cells transduced with pFUSPA-mArg-1-puro LV	C57BL/6J mice	Janvier, France

Table 3 - List of the primary and secondary antibodies used for western blot analyses

Antibody	Host	Working dilution	Catalog nr.	Company
Primary antibodies				
CatD	Goat	1:2000	6486	Santa Cruz, USA
Arg-1	Goat	1:1000	18354	Santa Cruz, USA
iNOS	Mouse	1:500	N6657	Sigma, Belgium
B-actin	Mouse	1:5000	47778	Santa Cruz, USA
Secondary antibodies				
Rabbit anti-goat HRP	Rabbit	1:1000	P0260	Dako, USA
Rabbit anti-mouse HRP	Goat	1:5000	P0449	Dako, USA

3.6. mRNA isolation, cDNA synthesis and qPCR

Quantitative PCR analysis was performed on IL-13 BMDMs (MOI of 36) and on BMDMs cultured with 100 µl conditioned media (CM) of IL-13 BMDMs to investigate the gene expression of M1 and M2 markers. Untreated BMDMs and rIL-13/LPS-stimulated BMDMs were used as controls. Total RNA of the cultured BMDMs was purified using the RNeasy Mini kit (Qiagen, Netherlands), according the manufacturer's instructions. The concentration and purity of the isolated RNA were evaluated by measuring the 260/280 nm ratio using a NanoDrop 2000 spectrophotometer (Isogen Life Science, The Netherlands). Total RNA was reverse transcribed into cDNA using qScript™ cDNA SuperMix (Quanta Biosciences, VWR, Belgium). Briefly, 200 ng of RNA was supplemented with 5x cDNA Supermix and nuclease-free water. The reverse transcription reaction was performed at 25°C for 5 min, 42°C for 30 min and 85°C for 5 min using the T100 Thermal Cycler (Bio-Rad Laboratories).

To perform quantitative PCR (qPCR) reactions, the cDNA (2,5 ng) was supplemented with fast SYBR Green master mix (Applied Biosystems, Belgium), gene-specific forward- (10 µM) and reverse primers (10 µM) and nuclease free water. The cDNA was amplified using a StepOnePlus detection system via a universal cycling program (20 sec at 95°C, 40 cycles of 3 sec at 95°C and 30 sec at 60°C). GeNorm software identified Cyclin A (CYCA) and hydroxymethylbilane synthase (HMBS) as most stable reference genes. Relative quantification of gene expression was accomplished by using the $2^{-\Delta\Delta CT}$ method. Data were normalized with CYCA and HMBS and expression levels were converted to fold change values versus the control. Primers used during qPCR analysis are shown below **(Table 4).**

Table 4 - List of the primers used for qPCR

Gene	Primer sequence (5'–3')
Cluster of differentiation 38 (CD38)	Forward: TGGGCCAGGTGTTTGGATTT Reverse AAATCCAAACACCTGGCCCA
Arginase-1 (Arg-1)	Forward: GTGAAGAACCCACGGTCTGT Reverse: GCCAGAGATGCTTCCAACTG
Inducible nitric oxide synthase (iNOS)	Forward: CCCTTCAATGGTTGGTACATGG Reverse ACATTGATCTCCGTGACAGCC
Chitinase-like 3 (Ym1)	Forward: CCACTGAAGTCATCCATGTC Reverse: GACATGGATGACTTCAGTGG
Formyl peptide receptor 2 (Fpr2)	Forward: TTACATCTACCACAATGTGAACTA Reverse: TAGTTCACATTGTGGTAGATGTAA
found in inflammatory zone 1 (Fizz1)	Forward: GGCCCATCTGTTCATAGTCTTGA Reverse: TCAAGACTATGAACAGATGGGCC
Cluster of differentiation 86 (CD86)	Forward: GAGCGGGATAGTAACGCTGA Reverse: GGCTCTCACTGCCTTCACTC
Cluster of differentiation 206 (CD206)	Forward: CTTCGGGCCTTTGGAATAAT Reverse: TAGAAGAGCCCTTGGGTTGA
G-protein coupled receptor 18 (Gpr18)	Forward: AGCGAGGCTTGGGTAAAACA Reverse: TGTTTTACCCAAGCCTCGCT

3.7. Enzyme-linked immunosorbent assay

Secretion of IL-13 in the medium of IL-13 BMDMs (MOI 36) was measured by using the mouse IL-13 ELISA Ready-SET-Go! kit (eBioscience, Austria) according to the manufacturer's instructions. Untreated BMDMs and rIL-13-stimulated BMDMs were used as controls.

3.8. Griess assay

Secretion of NO in the medium of IL-13 BMDMs (MOI 36) was measured by using the Griess Reagent System (Promega, USA), according to the manufacturer's instructions. Untreated BMDMs and rIL-13/LPS-stimulated BMDMs were used as controls.

3.9. Animal experiments

3.9.1. Animals and experimental groups

For all the *in vivo* experiments, the experimental set-up and the used mouse strains are enlisted in **table 5**. All mice were housed in a conventional animal facility at Hasselt University under standardized conditions, i.e. in a temperature-controlled room (20 ± 3°C) on a 12 h light-dark schedule and with food and water ad libitum. All experiments were approved by the local ethical committee of Hasselt University and they were performed according to the guidelines described in Directive 2010/63/EU.

Table 5 – Overview of all *in vivo* experiments performed during this study.

***In vivo* experiment**	**Experimental group**	**Control group**	**Mice/ Company**
Effect of catD inhibitors on functional recovery after SCI			
Inhibition by Pepstatin-A (pep-A)	Intrathecal injection of 0,25 µg/µl pep-A in a bolus of 200 µl NaCl from day 2-14 after inducing SCI	Intrathecal injection of 200 µl NaCl from day 2-14 after inducing SCI	9-11 weeks old female C57Bl/6J mice (Janvier, France)
Inhibition by pep-A + 3-methyladenine (3-MA)	Intraperitoneal injection of 0,25 µg/µl pep-A + 0,5 µg/µl 3-MA in a bolus of 200 µl NaCl/DMSO from day 1-14 after inducing SCI	Intrathecal injection of 200 µl NaCl/DMSO from day 1-14 after inducing SCI	9-11 weeks old female C57Bl/6J mice (Janvier, France)
Effect of plant sterols on functional recovery after SCI			
Using a Abcg5$^{-/-}$ animal model	Abcg5$^{-/-}$ mice, lack the abcg5 transporter and therefore they accumulate plant sterols in their body	Normal wild type mice	9-12 weeks old male C57Bl/6J mice (InnoSer, The Netherlands; Janvier, France)
Using a high plant sterol rich diet	WT mice were put on high PS rich diet 6 weeks pre- and 4 weeks post-injury	WT mice were put on a normal diet	9-12 weeks old male C57Bl/6J mice (Janvier, France)

3.9.2. Spinal cord T-cut hemisection injury

T-cut hemisection was performed as described previously (39). Briefly, mice were anesthetized with isoflurane (3%, IsoFlo, Abbot Animal Health, Belgium) and a partial laminectomy was performed at thoracic level T8 to expose the dorsal aspect of the spinal cord. Microscissors were used to transect the left and right dorsal funiculus, the dorsal horns and the ventral funiculus. This T-cut procedure results in the complete transection of the dorsomedial corticospinal tract (CST). Next, the muscles were sutured and the back skin was closed by wound clips (Autoclip®,Clay-Adams Co., Inc.). The aftercare included an intraperitoneal injection of 1 ml of glucose (20%) to compensate blood loss during the surgery and a subcutaneous injection of the analgesic buprenorphine (0.1 mg/kg, Temgesic®, Schering Plough). All mice were placed in heated recovery chambers (±33°C) until they regained their normal thermoregulation. Bladders were emptied manually, until the micturition reflex was recovered.

3.9.3. Assessment of functional locomotor recovery

The functional locomotor recovery of the animals is measured according to the Basso mouse scale (BMS) starting from day 1 until day 21 after SCI (40). The BMS is a 10-point locomotor rating scale, which measures locomotion, paw placement and trunk stability of mice in an open field during a 4-minute interval (9 = normal locomotion; 0 = complete hind limb paralysis). In the first week after injury, mice were scored daily. From the start of the second week until the end of the observation period, mice were examined every second day. Mice were scored by two investigators, blinded for the experimental conditions.

3.10. Statistical analysis

Statistical analysis was performed with GraphPad Prism version 5.01 (Graphpad software, USA). Data sets were analyzed for normal distribution using the D'Agostino-Pearson normality test. Only when $n \geq 3$, a statistical analysis was performed. The functional recovery *in vivo* was statistically analyzed using two-way analysis of variance (ANOVA) for repeated measurements, followed by Bonferroni post-hoc test for multiple comparisons. Western blot data were analyzed using the nonparametric Mann-Whitney U test. ELISA results were analyzed using the Kruskal-Wallis test, followed by Dunn's multiple comparison test. Data were presented as mean values ± standard error of the mean (SEM). Differences were considered significant when $p < 0.05$.

4. Results

4.1. Adoptive transfer of IL-13-overexpressing BMDMs to improve the functional recovery after SCI

4.1.1. BMDMs transduced with an IL-13 lentiviral vector secrete high levels of IL-13 and express both the IL-13Rα1 and IL-13Rα2 chain

BMDMs were transduced with an IL-13 LV (MOI 36) in order to obtain IL-13 BMDMs. To measure the secretion of the cytokine IL-13, culture medium of IL-13 BMDMs was analysed using ELISA. Results indicate that the conditioned media of the IL-13 BMDMs contain significantly more IL-13 compared to the other groups (IL-13 BMDMs: 973 ± 164,8 pg/ml IL-13, rIL-13-stimulated BMDMs: 146 ± 56,02 pg/ml IL-13, LPS-stimulated BMDMs: 7,366 ± 4,925 pg/ml IL-13 and untreated BMDMs: 2,002 ± 1,171 pg/ml IL-13) **(Figure 4A)**. Next, an immunofluorescence staining for both the IL-13Rα1 and IL-13Rα2 chain was performed on the BMDMs to investigate whether the produced IL-13 can induce autocrine effects. Fluorescent images reveal the presence of both the IL-13Rα1 and IL-13Rα2 chain on BMDMs **(Figure 4B)**. These data indicate that BMDMs transduced with an IL-13 LV effectively secrete IL-13. Moreover, it is possible that this produced IL-13 can induce autocrine effects by binding on the type I or type II IL-13R.

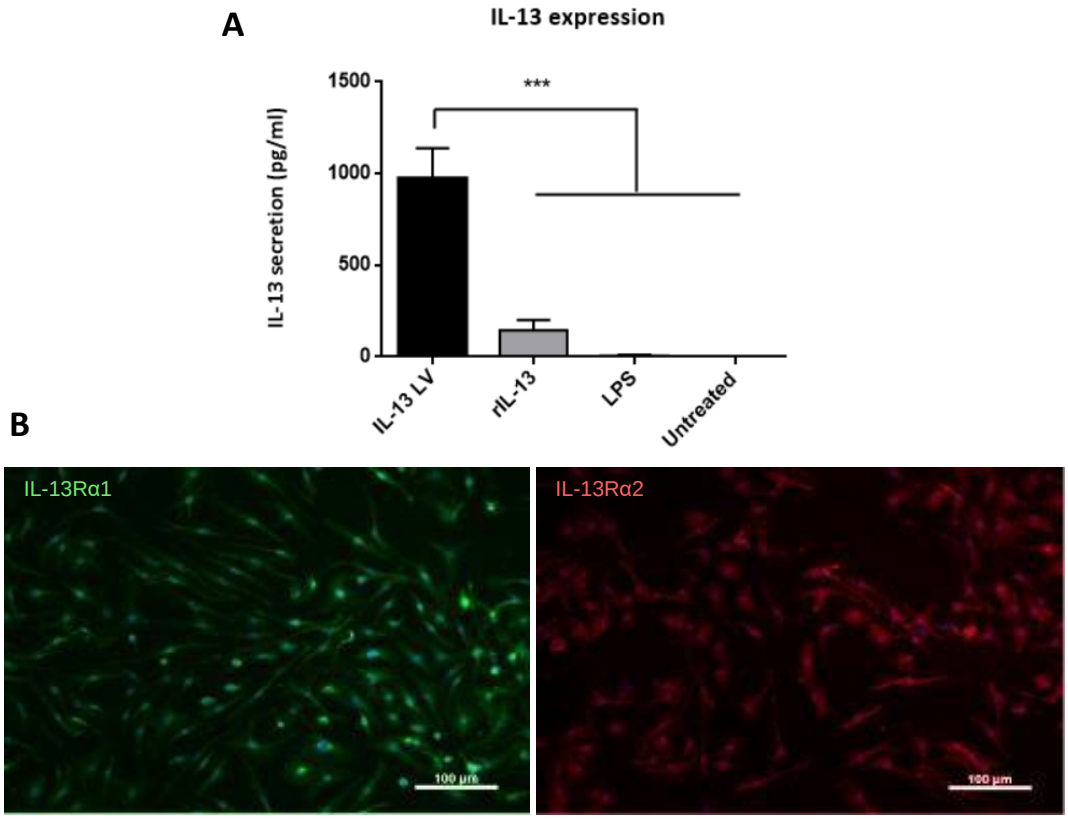

Figure 4: IL-13 BMDMs secrete upregulated levels of IL-13 compared to control BMDMs and express both the IL-13Rα1 and IL-13Rα2 chain. A) IL-13 levels in the culture medium of IL-13 BMDMs were measured by ELISA. IL-13 BMDMs transduced at a MOI of 36 secrete significantly more IL-13 compared to the other groups (IL-13 BMDMs: 973 ± 164,8 pg/ml IL-13, rIL-13-stimulated BMDMs: 146 ± 56,02 pg/ml IL-13, LPS-stimulated BMDMs: 7,366 ± 4,925 pg/ml IL-13 and untreated BMDMs: 2,002 ± 1,171 pg/ml IL-13). ELISA results are presented as mean values per group ± SEM; n = 3 per condition; *** p < 0,001. **B)** Immunofluorescence stainings were performed in order to investigate the presence of IL-13Rα1 and IL-13Rα2 on BMDMs. Both IL-13Rα1 (green) and IL-13Rα2 (red) are expressed. Nuclei were counterstained with DAPI (blue). One representative image is shown. Scale bars: 100 µm. BMDMs, bone marrow-derived macrophages; DAPI, 4',6-diamidino-2-phenylindole; ELISA, enzyme linked immunosorbent assay; IL-13, interleukin 13; IL-13Rα1, interleukin 13 receptor alfa 1; IL-13Rα2, interleukin 13 receptor alfa 2; LPS, lipopolysaccharide; LV, lentiviral vector; rIL-13, recombinant IL-13; VP, viral particles.

4.1.2. BMDMs transduced with an IL-13 lentiviral vector polarize towards an M2 phenotype

Subsequently, the phenotype of IL-13 BMDMs (MOI 36) was examined to investigate if they can alter their own phenotype via autocrine signalling pathways. Gene expression analysis was performed in order to identify the mRNA expression of classical M1 and M2 markers. Quantitative PCR analysis shows upregulated mRNA levels of Arg-1, CD206, Fizz and Ym1 in IL-13 BMDMs compared to untreated and LPS-stimulated BMDMs **(Figure 5A)**. The expression of M2 markers is higher or equal to the expression by rIL-13-stimulated BMDMs, which were used as a positive control for the M2 phenotype. On the other hand, we also investigated the gene expression of canonical M1 markers in all conditions. LPS-stimulated BMDMs, which were used as a positive control for the M1 phenotype, express upregulated mRNA levels of the M1 markers iNOS, CD38, CD86, Gpr18 and Fpr2, compared to the three other conditions **(Figure 5B)**.

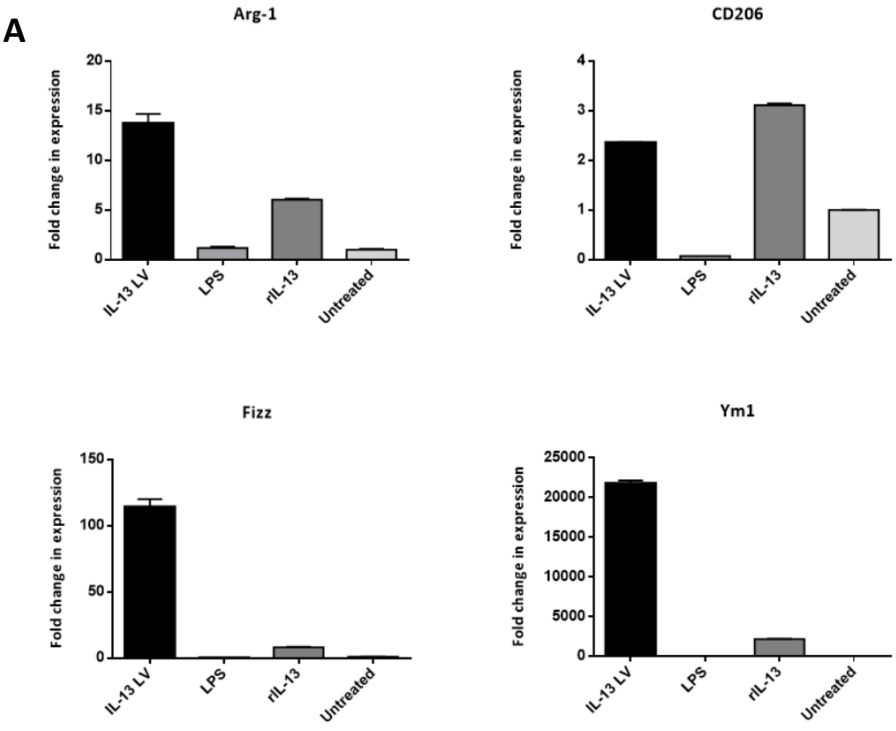

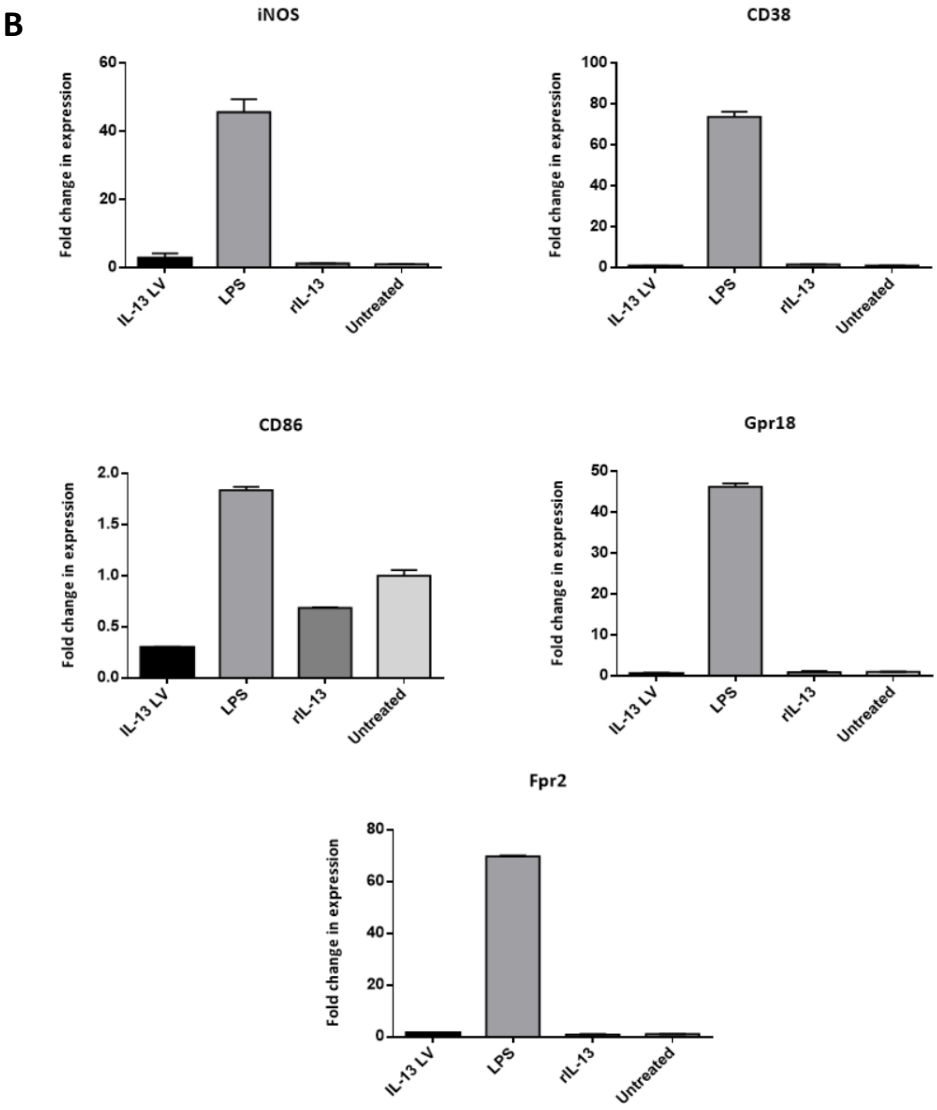

Figure 5: mRNA levels of M2 markers were upregulated in IL-13 BMDMs. The mRNA expression levels of M1 and M2 macrophage markers were measured in IL-13 BMDMs (MOI 36), LPS/rIL-13-stimulated BMDMs and untreated BMDMs. **A)** qPCR analysis shows upregulated mRNA levels of Arg-1, CD206, Fizz and Ym1 (M2 markers) in IL-13 BMDMs compared to LPS/rIL-13-stimulated and untreated BMDMs. **B)** In LPS-stimulated BMDMs, an increased mRNA expression is detected for the classical M1 markers (iNOS,CD38, Gpr18, CD86 and Fpr2) compared to other conditions. Expression levels were normalized to the reference genes: CYCA and HMBS. They are presented as fold change of the untreated condition. In each condition, to obtain the mRNA, 3 wells of 150 000 cells were pooled; n = 2 technical replicates per condition. Arg-1, arginase-1; BMDMs, bone marrow-derived macrophages; CD38, cluster of differentiation 38; CD86, cluster of differentiation 86; CD206, cluster of differentiation 206; Fizz, found in inflammatory zone 1; Fpr2, formyl peptide receptor 2; Gpr18, G-protein coupled receptor 18; IL-13, interleukin 13; IL-13 BMDMs, IL-13-overexpressing BMDMs; iNOS, inducible nitric oxide synthase; LPS, lipopolysaccharide; rIL-13, recombinant IL-13; Ym1, chitinase 3-like protein 3.

The M2 polarization after transduction has been confirmed at the protein level by a western blot analysis. IL-13 BMDMs display an increased Arg-1 expression compared to rIL-13-stimulated BMDMs and untreated BMDMs **(Figure 6A)**. iNOS expression is only observed in LPS-stimulated BMDMs. Next, a Griess assay was performed. High levels of NO are measured in the medium of LPS-stimulated BMDMs (7,722 ± 0,2776 µM) whereas only limited NO expression levels are observed in IL-13 BMDMs (0,8062 ± 0,4735 µM), rIL-13-stimulated BMDMs (0,0582 ± 0,0203 µM) and untreated BMDMs (0,2220 ± 0,2021 µM) **(Figure 6B)**.

The macrophage M2 polarization was further confirmed via flow cytometry analysis by measuring CD206 **(Figure 6C)** and Arg-1 levels **(Figure 6D)**. IL-13 BMDMs show a substantial increased CD206 (39,9%) and Arg-1 (48,9%) protein expression, compared to the untreated BMDMs (CD206: 0%; Arg-1: 0,9%) and LPS-stimulated BMDMs (CD206: 29,9%; Arg-1: 6,1%). rIL-13 BMDMs have an increased CD206 expression (63,4%), while having a decreased Arg-1 expression (21%) compared to IL-13 BMDMs. Taken together, these results indicate that IL-13 BMDMs secrete functional IL-13 which polarizes IL-13 BMDMs towards an M2 phenotype via autocrine signaling mechanisms.

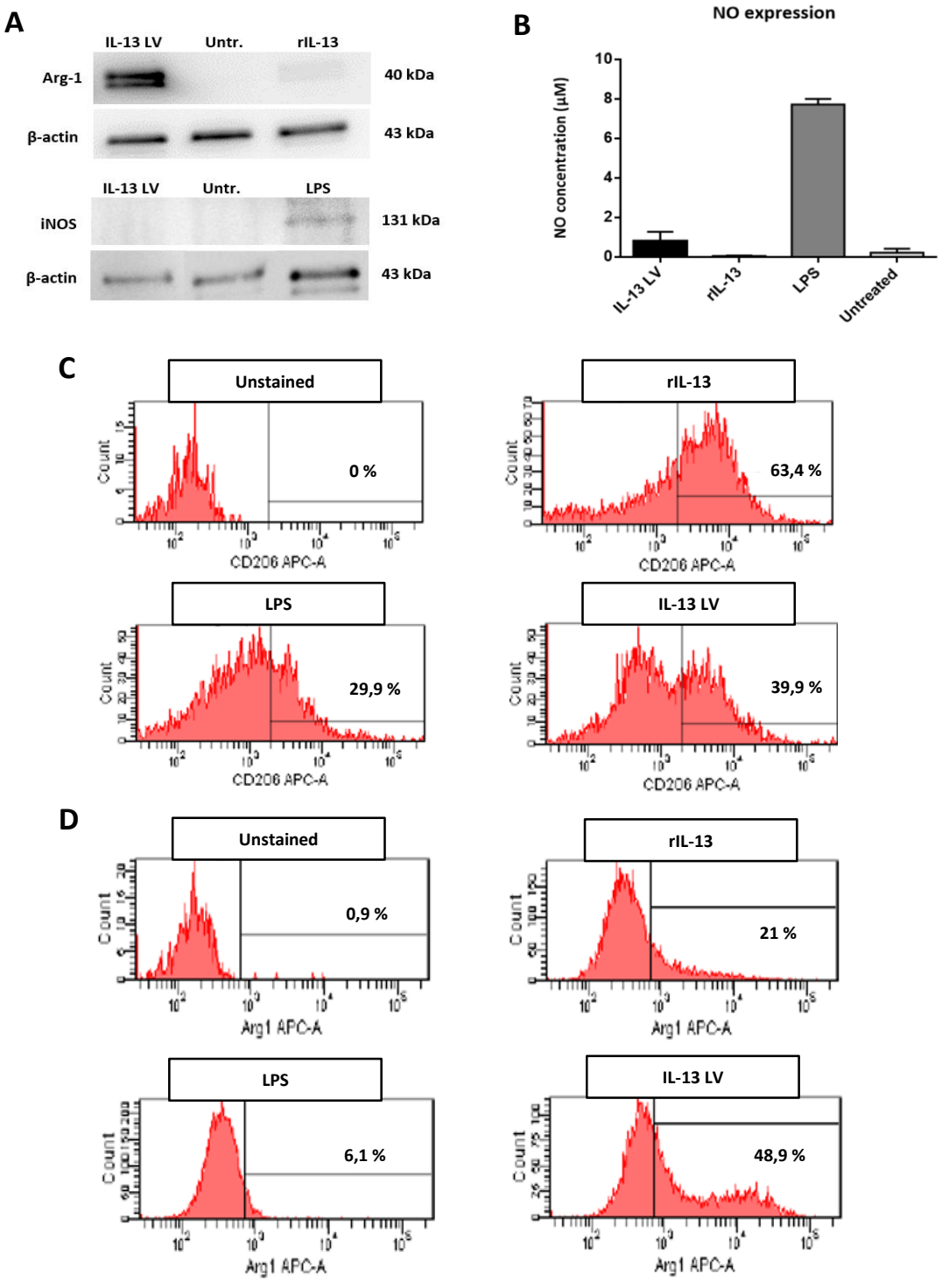

Figure 6: IL-13 BMDMs obtain an M2 phenotype via IL-13 autocrine signaling mechanisms. To investigate the phenotype of IL-13 BMDMs, the expression of different M1 and M2 phenotype markers was investigated and compared to those of untreated BMDMs and BMDMs stimulated with LPS/rIL-13. **A)** Western blot analysis shows an increased Arg-1 expression in IL-13 BMDMs, compared to untreated or rIL-13-stimulated BMDMs. iNOS expression is only observed in LPS-stimulated BMDMs. One representative image is shown; n = 3 per condition. **B)** Levels of NO secretion were analysed by performing a Griess assay. In LPS-stimulated BMDMs, which are used a positive control for M1 macrophages, the NO expression (7,722 ± 0,2776 µM) is higher compared to the NO expression of IL-13 BMDMs (0,8062 ± 0,4735 µM), rIL-13 -stimulated BMDMs (0,0582 ± 0,0203 µM) and untreated BMDMs (0,2220 ± 0,2021 µM). The results are presented as mean values per group ± SEM; n = 2 per condition. **C-D)** Flow cytometry shows upregulated protein levels of CD206 **(C)** and Arg-1 **(D)** in IL-13 BMDMs compared to LPS-stimulated and untreated BMDMs. In each condition, 3 wells of 150 000 cells were pooled; n = 1 per condition. Arg-1, arginase-1; β-actin, beta-actin; BMDMs, bone marrow-derived macrophages; CD206, cluster of differentiation 206; IL-13, interleukin 13; kDa, kilo Dalton; LPS, lipopolysaccharide; LV, lentiviral vector; NO, nitric oxide; rIL-13, recombinant IL-13; VP, viral particles.

4.1.3. Conditioned media of IL-13-overexpressing BMDMs polarize M0 macrophages towards an M2 phenotype

Next, the paracrine effects of IL-13 secreted by IL-13 BMDMs were investigated. M0 macrophages were cultured with the conditioned media (CM) derived from IL-13 BMDMs and analyzed for their gene expression of specific M1 and M2 phenotype markers. After a 48h incubation period, the expression of all M2 markers (Arg-1, CD206, Fizz and Ym1) are upregulated in macrophages cultured with the CM, compared to all other conditions **(Figure 7A)**. On the other hand, the mRNA levels of M1 markers, such as iNOS, CD38, Fpr2, CD86 and Gpr18 are similar among untreated, rIL-13 and CM-treated BMDMs. LPS-stimulated BMDMs display elevated mRNA levels of M1 markers compared to the other three groups **(Figure 7B)**. These results indicate that the IL-13 secreted by IL-13 BMDMs can polarize naïve macrophages towards an M2 phenotype. This was further confirmed by western blot analysis which reveals high Arg-1 protein expression levels in BMDMs cultured with the CM and rIL-13-stimulated BMDMs **(Figure 7C)**. No Arg-1 expression was observed in LPS-stimulated and untreated BMDMs. Only in LPS-stimulated BMDMs an iNOS expression is detected.

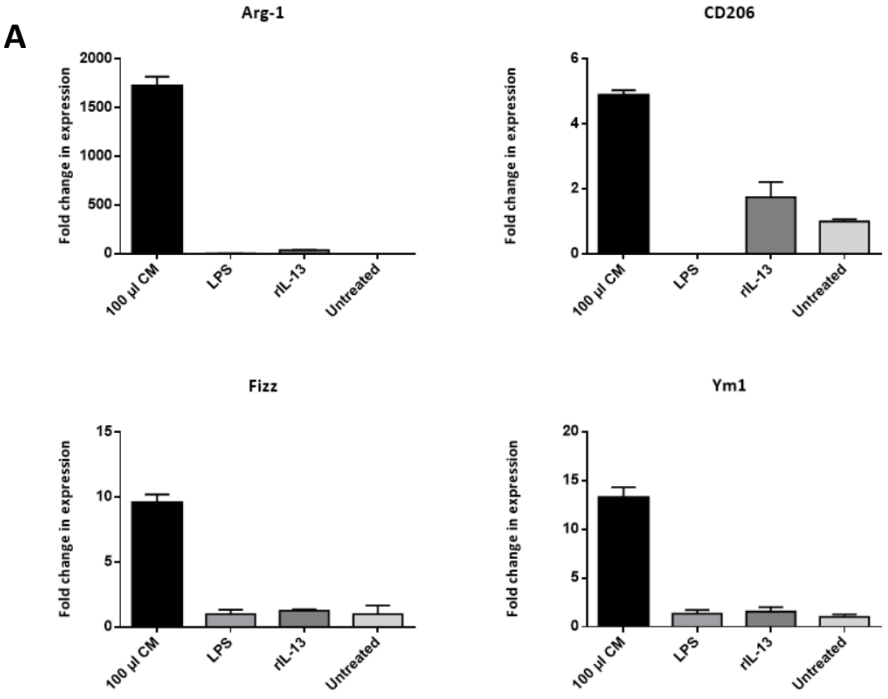

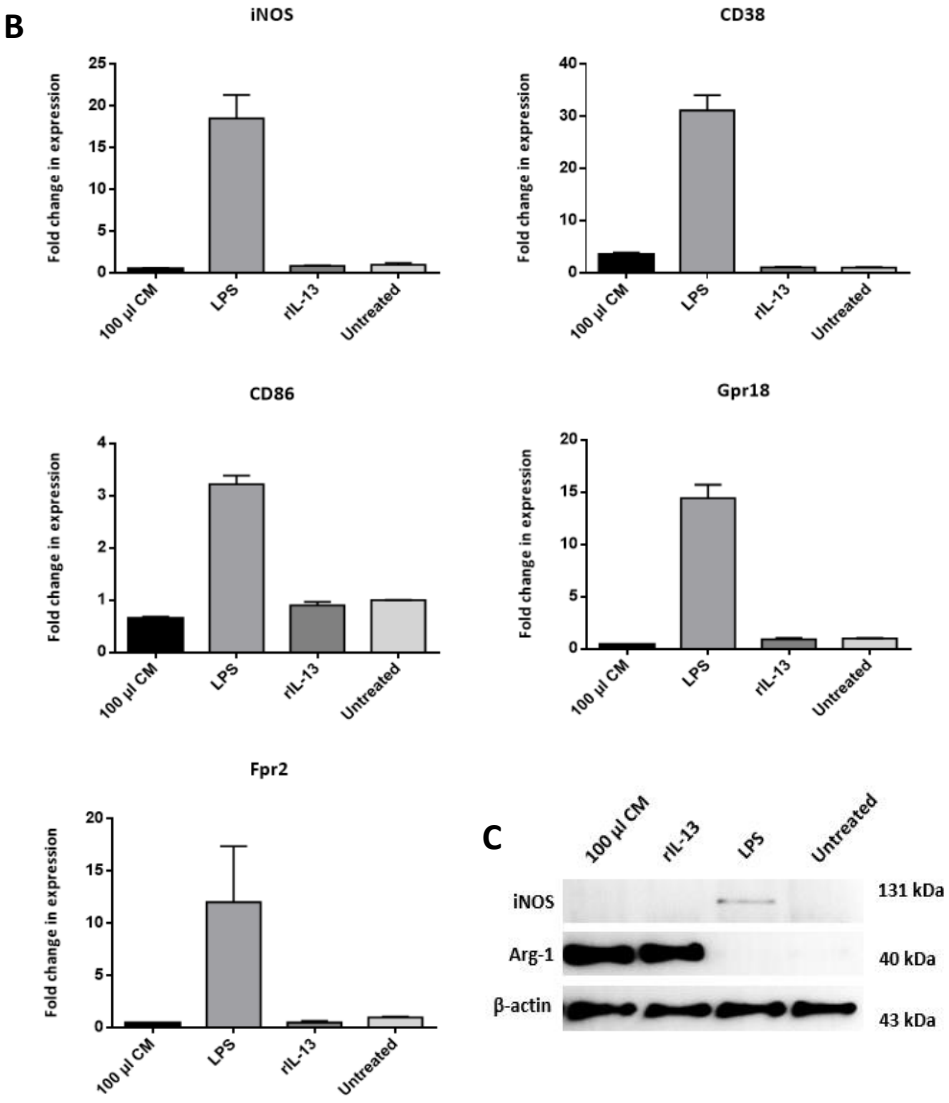

Figure 7: Conditioned media of IL-13 BMDMs can polarize naïve macrophages towards an M2 phenotype. The mRNA expression levels of M1 and M2 markers were measured in BMDMs cultured with 100 µl CM from IL-13 BMDMS (MOI 36), LPS-stimulated BMDMs, rIL-13-stimulated BMDMs and untreated BMDMs. **A)** After a 48h incubation period, the expression of all M2 markers (Arg-1, CD206, Fizz and Ym1) are upregulated in macrophages cultured with the CM, compared to all other conditions. **B)** In LPS-stimulated BMDMs an increased mRNA expression is observed for the classical M1 markers iNOS, CD38, Gpr18, CD86 and Fpr2, compared to other conditions. Expression levels were normalized to the reference genes: CYCA and HMBS. They are presented as fold change of the untreated condition. In each condition, to obtain the mRNA, 3 wells of 150 000 cells were pooled; n = 2 technical replicates per condition. **C)** Western blot analysis indicated increased Arg-1 protein levels in BMDMs cultured with CM and rIL-13 BMDMs compared to untreated and LPS-stimulated BMDMs. Only in LPS-stimulated BMDMs an iNOS expression is observed. One representative image is shown; n = 2 per condition. Arg-1, arginase-1; β-actin, beta-actin; BMDMs, bone marrow-derived macrophages; CD38, cluster of differentiation 38; CD86, cluster of differentiation 86; CD206, cluster of differentiation 206; CM, conditioned media; Fizz, found in inflammatory zone 1; Fpr2, formyl peptide receptor 2; Gpr18, G-protein coupled receptor 18; IL-13, interleukin 13; IL-13 BMDMs, IL-13-overexpressing BMDMs; iNOS, inducible nitric oxide synthase; kDa, kilo Dalton; LPS, lipopolysaccharide; rIL-13, recombinant IL-13; Ym1, chitinase 3-like protein 3.

4.2. Construction of the arginase-1 lentiviral vector

In BMDMs, Arg-1 lowers the toxic NO production and stimulates axonal growth via production of polyamines. Therefore, we hypothesize that the functional recovery after SCI will be improved by adoptive transfer of Arg-1-overexpressing BMDMs. The goal for this master thesis project is to produce stable and functional Arg-1 lentiviral vector particles which are able to transduce BMDMs, resulting in Arg-1-overexpressing BMDMs. The following chapter includes a methodology for the construction of a pFUSPA-Arg-1-puro plasmid and a pFUSPA-Arg-1-puro lentiviral vector.

4.2.1. Construction of the pFUSPA-Arg-1-puro plasmid using PCR-based cloning

PCR-based cloning was used to copy Arg-1 cDNA from the pcDNA3, 1-mArg-1 plasmid and to add Asc-1 restriction sites flanking the Arg-1 DNA, so that it can be easily cloned into the recipient vector pFUSPA-puro. In a following step, Asc-1 restriction digestion was performed on both the purified PCR product and the empty pFUSPA-puro plasmid. Agarose gel electrophoresis of the restriction products reveals that the digested pFUSPA-puro plasmid has an increased base pair length compared to the undigested pFUSPA-puro. This indicates a successful Asc-1 restriction digestion because undigested DNA has a circular conformation, while digested DNA has a linear conformation, resulting in an increased resistance during gel electrophoresis **(Figure 8A)**.

After confirming a successful Asc-1 restriction digestion, ligation of the amplified Arg-1 cDNA into the digested pFUSPA-puro plasmid was performed. This was possible because the pFUSPA-puro plasmid contained an Asc-1 restriction site in its multiple cloning site. However, the Arg-1 cDNA can be inserted in either the right or the false orientation in the pFUSPA-puro plasmid. To check the correct orientation of the construct, competent *E.coli* were transformed with 1-2 µl of the ligation reaction and grown on LB-agar culture plates. Five colonies were picked and checked for successful ligations by performing a XhoI restriction analysis **(Figure 8B)**. This restriction enzyme was chosen because it cuts the pFUSPA-mArg-1-puro plasmid one time in the Arg-1 sequence and one time in a non-coding region. Based on the orientation of Arg-1 cDNA into the pFUSPA-mArg-1-puro plasmid, two different fragment sizes arise, which makes it possible to select the pFUSPA-mArg-1-puro plasmid with the correct Arg-1 cDNA orientation. For the correct orientation, XhoI restriction analysis results in a short fragment of 2767 bp and a long fragment of 8651 bp (indicated by red box). Contrarily, if the Arg-1 cDNA has an opposite orientation, XhoI restriction results in a short fragment of 1917 bp and a long fragment of 9501 bp. Next, HEK293T cells were transfected with the pFUSPA-mArg-1-puro plasmid, isolated from the colony where it was assumed the construct had the correct orientation. A western blot analysis for Arg-1

expression was performed on these transfected HEK293T cells to check the functionality of the pFUSPA-mArg-1-puro plasmid. An upregulated Arg-1 protein expression is observed in the transfected HEK293T cells compared to control HEK293T cells **(Figure 8C)**. This expression pattern is similar to the Arg-1 expression in IL-13 BMDMs, which was used as positive control. Finally, sequencing analysis was performed to confirm the correct orientation of the Arg-1 cDNA insert.

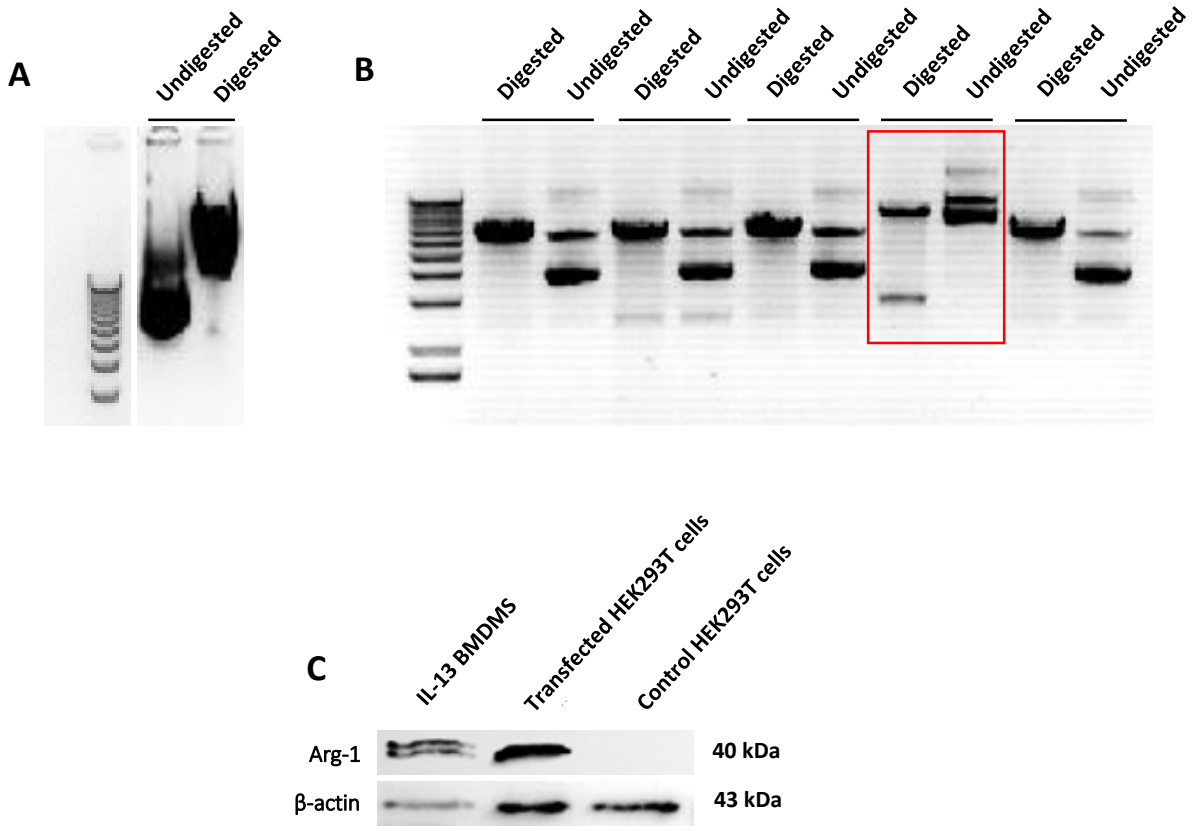

Figure 8: construction of pFUSPA-Arg-1-puro plasmid. A) An Asc-1 restriction digestion of pFUSPA-puro was performed. Both digested and undigested pFUSPA-puro were analyzed via gel electrophoresis to check the functionality of the Asc-1 restriction enzyme. **B)** Competent *E.coli* were transformed with the ligation reaction. Five colonies were picked and checked for successful ligations by performing a XhoI restriction analysis. The fourth colony that was tested, contains the pFUSPA-mArg-1-puro plasmid with the correct Arg-1 cDNA orientation (indicated by red box). **C)** HEK293T cells were transfected with the pFUSPA-mArg-1-puro plasmid and analyzed on their Arg-1 expression via western blot analysis. IL-13 BMDMs and untransfected HEK293T cells were used as positive and negative control, respectively. Results indicate an increased Arg-1 expression in the HEK293T cells transfected with the pFUSPA-mArg-1-puro plasmid compared to control conditions. Arg-1, arginase-1; β-actin, beta-actin; HEK293T cells, human embryonic kidney cells; IL-13 BMDMs, IL-13-overexpressing BMDMs; kDa, kilo Dalton.

4.2.2. Production of pFUSPA-Arg-1-puro lentiviral vector particles

Lentivirus became one of the most popular tools for gene delivery, which can transduce both dividing and non-dividing cells. They permit long-term transgene expression by integrating into the host genome. During this protocol, lentiviral particles are produced by HEK293T cells, using a second generation lentiviral system.

When HEK293T cells reached a confluency of 85 – 90%, they were transfected with the plasmid mix containing the transfer vector pFUSPA-Arg-1-puro plasmid, the packaging plasmid (psPAX) and the envelop plasmid (pMDG2). One week after transfection, the medium contained the pFUSPA-Arg-1-puro LV particles. To investigate the transduction potential of the produced pFUSPA-Arg-1-puro LV particles, HEK293T cells were transduced with these lentiviral particles and analyzed for their Arg-1 protein expression. Western blot analysis indicates an upregulated Arg-1 expression in HEK293T cells transduced with the pFUSPA-Arg-1-puro LV compared to negative controls (HEK293T cells transduced with an empty pFUSPA-puro LV or untransduced HEK293T cells) **(Figure 9)**. Hence, these data indicate that the produced lentiviral particles were able to effectively transduce HEK293T cells and induce an upregulated Arg-1 expression.

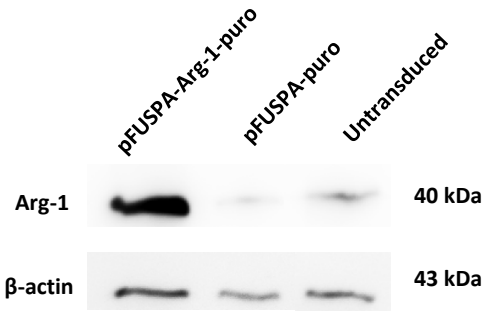

Figure 9: Transduction of HEK293T cells with pFUSPA-Arg-1-puro LV. Western blot analysis was performed on HEK293T cells transduced with an pFUSPA-Arg-1-puro LV. HEK293T cells transduced with an empty pFUSPA-puro or untransduced HEK293T cells were used as negative control. Western blot analysis indicates an upregulated Arg-1 expression in HEK293T cells transduced with the pFUSPA-Arg-1-puro LV compared to negative controls. Arg-1, arginase-1; β-actin, beta-actin; HEK293T cells, human embryonic kidney cells; kDa, kilo Dalton; Lentiviral vector, LV.

4.3. Targeting cathepsin D to improve the functional recovery after SCI

4.3.1. SCI results in an upregulated expression of cathepsin D

To investigate protein expression patterns of catD in mice at different time points after SCI (day 1, 4, 7 and 10 post-injury), a western blot analysis was performed on spinal cord lysates. Local intermediate catD protein levels are significantly increased at day 4 after SCI, followed by a decrease to basal levels at day 7 and 10 post-injury **(Figure 10)**. This increase was only found after inducing a T-cut hemisection SCI and not in sham-operated mice (laminectomy). Subsequently, upregulated levels of mature catD protein levels are observed from day 4 until day 10 after SCI compared to sham-operated mice. However, these differences did not reach statistical significance. These data indicate that both intermediate- and mature catD protein levels are upregulated in the injured spinal cord.

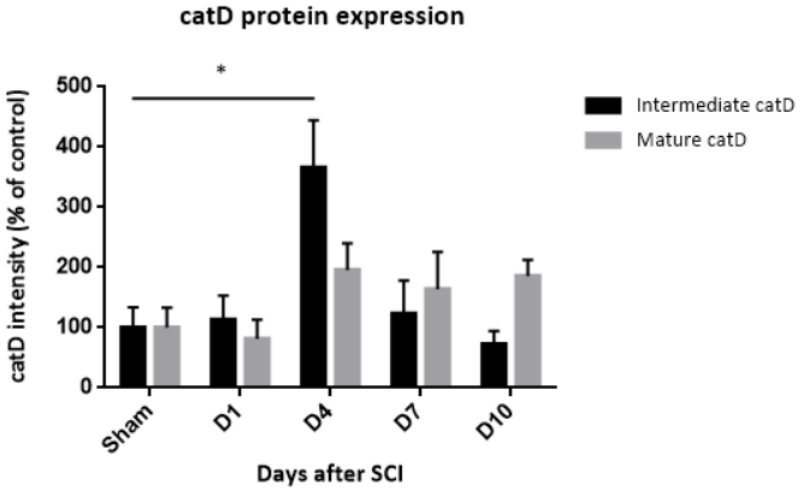

Figure 10: CatD protein levels were increased after inducing SCI in mice. A western blot analysis was performed to investigate catD protein levels during different time points after SCI. Peak intermediate catD protein levels are observed at day 4 post-injury, while mature catD protein levels are increased from day 4 until day 10 post-injury compared to the sham-operated mice (laminectomy). Data are presented as mean values normalized to the control ± SEM; n = 3-4 for each time point; * $p < 0,05$ compared to sham-operated mice. catD, cathepsin D; D, Day; SCI, spinal cord injury.

4.3.2. Inhibition of both intra- and extracellular cathepsin D does not affect the functional outcome after SCI

Now that we know that the catD levels are significantly increased at the lesion site of SCI mice, a next step is to investigate if catD inhibitors have the potential to improve the functional recovery after SCI by reducing the catD concentration back to basal levels. Therefore, the functional recovery of SCI mice was analysed after administration of catD inhibitors according to the BMS scale from day 1 until day 28 post-injury. In a first *in vivo* experiment, we aimed to block the intracellular neurotoxic pathway of catD by injecting pep-A. NaCl was injected in the vehicle control group. No significant differences are observed in the functional recovery between both groups. **(Figure 11A)**.

Besides intracellular catD, also extracellular catD can induce neurotoxicity. Therefore, in a second *in vivo* experiment, both intra-and extracellular neurotoxic pathways of catD were blocked by injecting pep-A in combination with 3-MA. In the vehicle control group, mice were injected with NaCl/DMSO. BMS scores reveal no significant differences in locomotion between mice treated with the combination therapy and control mice **(Figure 11B)**. Taken together, our results suggest that both catD inhibitors peps-A and 3-MA are not sufficient to improve the functional recovery after SCI.

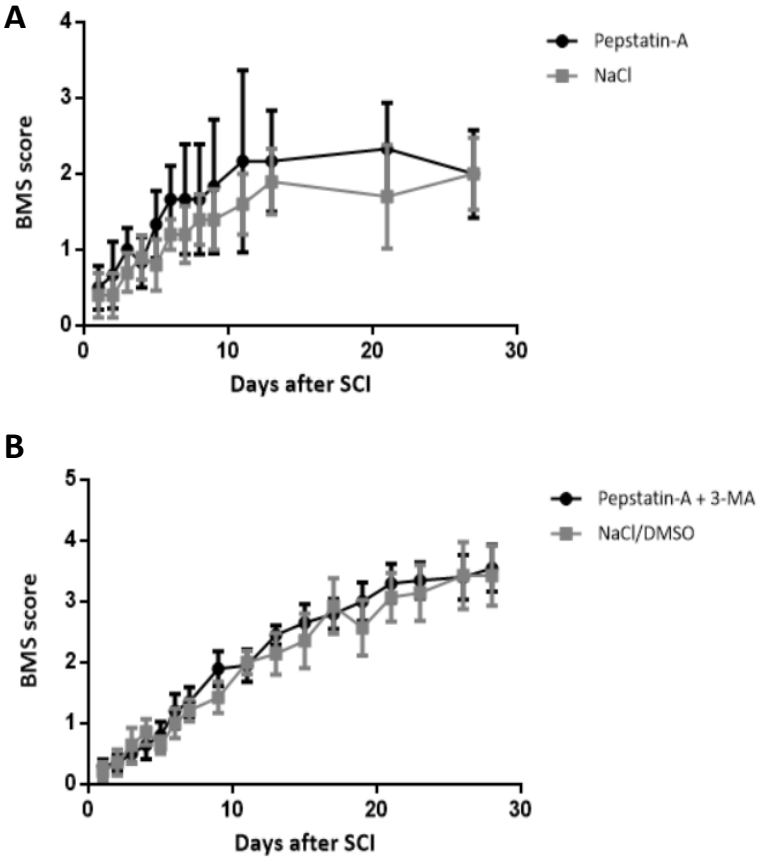

Figure 11: CatD inhibitors do not affect the functional recovery after SCI. A T-cut hemisection was performed to induce SCI in the mouse model. Recovery of hind limb movements was measured according to the BMS scale. **A)** From day 2 – 14 after inducing SCI, mice of the experimental group were intrathecally injected with pep-A (2,5 mg/kg) or with the vehicle NaCl. No significant differences are observed in the functional recovery between both groups. n = 3 - 5 per condition. **B)** From day 1 – 14 after inducing SCI, mice were intraperitoneally injected with a combinational therapy, containing pep-A (2,5 mg/kg) and 3-MA (5mg/kg). Mice in the control group were intraperitoneally injected with NaCl/DMSO as vehicle control. The BMS scores do not significantly differ between both groups. Results are presented as mean values per group ± SEM; n = 6 – 10 per condition. 3-MA, 3-methyladenine; BMS, Basso Mouse Scale; CatD, cathepsin D; SCI, spinal cord injury; DMSO, dimethyl sulfoxide; NaCl, sodium chloride; Pep-A, pepstatin-A.

4.4. The effect of plant sterols on the regenerative process after SCI

4.4.1. Plant sterols have no influence on the functional recovery after SCI

Since many articles highlight the beneficial anti-inflammatory effects of PS in the CNS, we have investigated the effects of these PS on the functional recovery after SCI. Therefore, we used two different animal models with elevated blood PS levels, namely the Abcg5$^{-/-}$ mice and mice fed a high PS rich diet. After inducing SCI, the functional recovery was measured according to the BMS. In a first *in vivo* experiment, the functional outcome of the experimental group (Abcg5$^{-/-}$ mice) was compared to that of wildtype mice, until 21 days post-injury. According to the BMS data, the locomotor performance of Abcg5$^{-/-}$ mice is lower compared to the control group, although the observed differences do not reach statistical significance **(Figure 12A)**. In a second *in vivo* experiment, the locomotor recovery of mice fed with a high PS rich diet was compared to those of mice put on a normal diet. No significant differences in locomotor function are observed between both groups **(Figure 12B)**. These data reveal that high levels of PS do not improve the functional recovery after SCI.

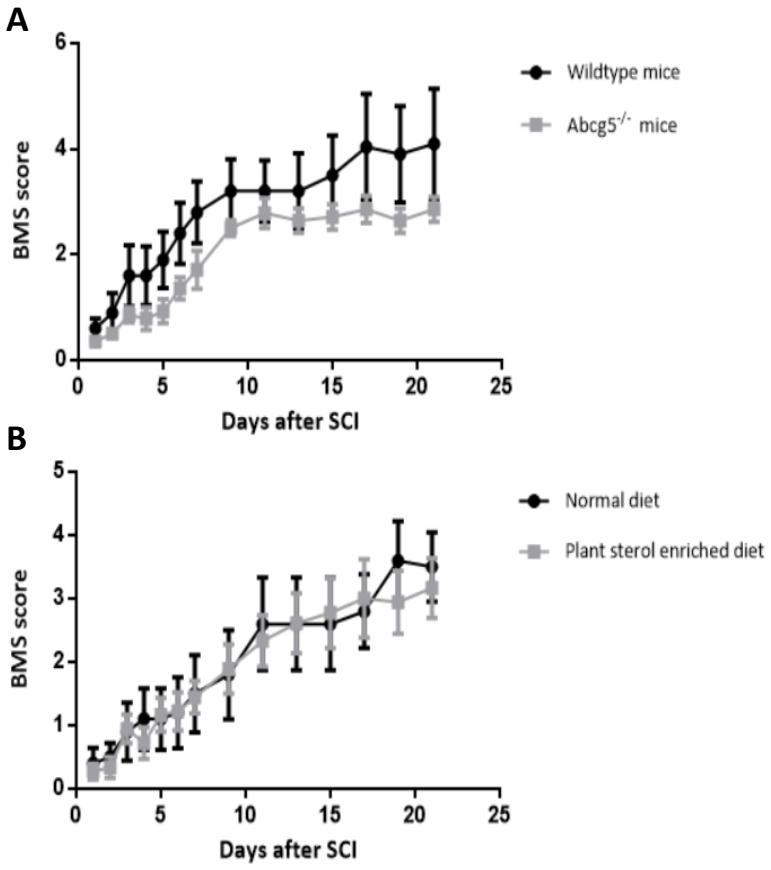

Figure 12: Plant sterols do not improve the functional recovery after SCI. After inducing a T-cut hemisection, the recovery of hind limb movements was measured according to the BMS scale. **A)** The BMS score reveals less, although not significant, functional recovery of the Abcg5$^{-/-}$ mice compared to control mice. **B)** Mice in de experimental group were put on a high PS rich diet 6 weeks pre- and 3 weeks post-injury, whereas control mice were fed with normal food. No significant differences in locomotor function are observed between both groups. Results are presented as mean values per group ± SEM; n = 5-9 per condition. Abcg5$^{-/-}$, ATP-binding cassette sub-family G member knockout; BMS, Basso Mouse Scale; SCI, spinal cord injury.

5. Discussion

SCI is a disabling condition, leading to the loss of motor, sensory and autonomous functions below the lesion site. Since the CNS has a limited intrinsic ability to regenerate, most neurological disorders associated with SCI are severe and permanent. This failure of regeneration is partly due to inflammatory and neurotoxic processes present at the SCI lesion, causing a growth-inhibitory microenvironment. As a result, modulating this growth-inhibitory environment after SCI is a promising strategy to promote tissue repair after CNS injury. Therefore, we investigated different approaches targeting both the detrimental inflammatory and neurotoxic processes in order to create a more permissive environment for axonal regeneration after SCI.

5.1. Adoptive transfer of IL-13-overexpressing BMDMs to improve the functional recovery after SCI

The Inflammatory response is a key mediator of the secondary injury cascade following SCI. Different subtypes of immune cells infiltrate the injured CNS, playing distinct roles in either neuroprotection or neurotoxicity. Moreover, it is the balance between these subtypes that eventually regulates the functional outcome after SCI (41). This is exactly the problem during the SCI pathology. A rapid and prolonged M1 macrophage onset overwhelms the limited and transitory M2 macrophage response (13). In a previous study of Hu *et al.*, passive immunization of T-cells activated by myelin basic protein stimulated polarization of endogenous macrophages/microglia towards an M2 phenotype *in vivo*, resulting in an improved functional repair after SCI (42). However, clinical applications were unfeasible given the fact that three weeks are needed to activate these T-cells by myelin basic proteins, which is far outside the optimal time window for cell-transfer (1- to 2- week post-injury) (43). Moreover, transferred cells would not reach the SCI lesion site, since the BBB closes at three weeks post-injury (12). Although increasing the M2 population during SCI seems like an accessible treatment strategy, more research is needed to create feasible and effective ways to fulfill this task which eventually could be translated into clinical applications.

Therefore, the goal of this project was to investigate if IL-13-overexpressing BMDMs can polarize themselves (autocrine signaling) and other macrophages (paracrine signaling) towards an M2 phenotype by producing functional IL-13. Eventually, these IL-13 BMDMs will be administered to SCI mice and analyzed for their potential to improve the functional recovery after SCI. Initially, BMCs were isolated from the bone marrow of mice and cultured for eight days in standard culture medium supplemented with LCM-medium. The obtained BMDMs were defined as unpolarized (M0)

macrophages. Next, BMDMs were lentivirally transduced with an IL-13 vector to create IL-13-overexpressing BMDMs. Earlier findings of Lingbing *et al.* indicated that BMDMs were consistently more susceptible to viral vector-mediated gene transfer, compared to other types of macrophages, which supported our choice to use BMDMs during this study (44). ELISA revealed an upregulated IL-13 secretion in the conditioned media of IL-13 BMDMs compared to control BMDMs. Since IL-13 is a well-described M2 polarizing factor, we analyzed the expression of both the IL-13Rα1 and IL-13Rα2 chain on BMDMs to investigate if the secreted IL-13 could induce autocrine polarization effects (11). Fluorescence images revealed the presence of both the IL-13Rα1 and IL-13Rα2 chain on BMDMs. This was according to the literature, since many research groups already showed the expression of both the IL-13R subtypes on a lot of immune cells, including macrophages (15). These results suggested that IL-13 BMDMs can alter their own phenotype towards M2 via autocrine signaling pathways of IL-13.

To confirm this objective, we investigated the phenotype of IL-13 BMDMs by performing a gene expression analysis for specific M1 and M2 markers. Increased expression levels of the M2 markers (Arg-1, CD206, Fizz and Y1m) in IL-13 BMDMs indicated a polarization towards an M2 phenotype. Only in LPS-stimulated BMDMs, which were used as positive controls for the M1 phenotype, an upregulated expression of M1 markers (iNOS, CD38, CD86, Gpr18 and Fpr2) was observed. The M2 phenotype of IL-13 BMDMs was further confirmed at the protein level. IL-13 BMDMs expressed high levels of the well-known M2 marker Arg-1. However, rIL-13-stimulated BMDMs, which were used as positive controls for the M2 phenotype, had a low Arg-1 protein expression compared to IL-13 BMDMs. This can be explained by the fact that transduced BMDMs keep secreting high levels of IL-13 during time, while rIL-13 stimulated BMDMs consume rIL-13 without secreting it. This can result in a lower M2 polarization rate or even an repolarization towards an M0 or M1 phenotype.

Furthermore, an upregulated NO expression was observed in LPS-stimulated BMDMs. This is in line with our previous findings that iNOS is only expressed in LPS-stimulated BMDMs. Low NO secretion levels in the culture media of IL-13 BMDMs were expected since no iNOS expression was observed in these IL-13 BMDMs. Moreover, iNOS has to compete with Arg-1 for the L-arginine substrate to produce NO (28). As a result, high Arg-1 protein levels in IL-13 BMDMs decrease the available L-arginine for iNOS resulting in low NO production. These data showed that IL-13 BMDMs were polarized towards an M2 phenotype *in vitro* via autocrine signaling mechanisms of IL-13. These results were expected since previous studies already identified IL-13 as one of the most effective cytokines to generate alternatively active macrophages (18). Furthermore, our data revealed that IL-13 secreted by IL-13 BMDMs was not only able to polarize themselves, but also naïve macrophages towards an M2 phenotype *in vitro*. Taken together, these data suggest that IL-13 BMDMs are able to create an IL-13-

enriched environment, polarizing macrophages towards an M2 phenotype. However, it has to be noted that the results are preliminary and more experiments are necessary to validate our hypothesis.

Recently, also the immunomodulatory effects of IL-13 *in vivo* were described by Hoornaert *et al.* It is known that allogeneic MSC grafts are often rejected after transplantation by the host's immune system. Therefore, in this study they genetically modified MSCs with an IL-13 lentiviral vector and transplanted IL-13-overexpressing MSC allografts in the muscle tissue of mice to investigate the effect of IL-13 on MSC allograft rejection (45). They revealed that local secreted IL-13 modulates the allograft-specific immunity by inducing an M2 polarization in macrophages infiltrating the graft. This resulted in a prolonged survival of the allogeneic MSC graft. These data indicate that IL-13 is able to polarize endogenous macrophages *in vivo* towards an M2 phenotype. This makes IL-13 an interesting therapeutic agent for SCI since it can modulate the M1 macrophage population present after SCI. Nevertheless, during this project, we have chosen to investigate the effect of IL-13-overexpressing BMDMs during SCI instead of IL-13-overexpressing MSCs. This because previous studies have reported an increased potential for tumor formation in the CNS when using stem cells (46). Moreover, it has been shown that BMDMs can actively migrate to the SCI lesion site (47). This is an important factor since the goal of our study is the create a specific IL-13-enriched microenvironment at the SCI lesion site which primes macrophages towards an M2 phenotype.

Subsequently, a next step in our study is to investigate the potential of IL-13 BMDMs to improve the functional recovery in SCI mice to reveal their clinical potential. Increasing the M2 macrophage population in the SCI lesion site creates a microenvironment that is conducive for axon regeneration and residual myelin preservation. Recently, Ma *et al.* have observed a decreased spinal cord lesion volume and increased preservation of axon myelination after adoptive transfer of *in vitro* M2 polarized macrophages in SCI rats (12). However, in the literature, it has been reported that the lesion microenvironment is rich in M1 polarizing factors, favoring macrophage polarization towards an M1 phenotype. Moreover, even though an M2 macrophage onset was observed directly after SCI, this was short-lived, dissipating within 3-7 days post-injury (48). This was in line with findings of Kigerl *et al.*, who injected $EGFP^+$ M2 macrophages into SCI mice to investigate the effects of the lesion microenvironment on macrophage polarization. Three days post-injection, confocal microscopy revealed that only 20-40% of the injected cells maintained their M2 phenotype (13). Therefore, although Ma *et al.* observed an improved functional recovery, we believe that a substantial amount of the injected M2 macrophages were repolarized towards an M1 phenotype because of the typical lesion microenvironment. For that reason, we will inject IL-13-overexpressing BMDMs because besides themselves being M2, these macrophages can modulate the typical M1-polarizing environment by

secreting large amounts of IL-13. Eventually, the sustained IL-13 production at the lesion site may also prevent endogenous and infiltrating macrophages to obtain an M1 phenotype.

We have chosen to use *in vitro* transduced BMDMs which overexpress IL-13, instead of a direct local injection of lentiviral vectors. The latter would result in a random integration in the DNA of a broad range of cells after administration (49). Transplantation of genetically engineered BMDMs provides an opportunity for controlled IL-13 production at the lesion site. Moreover, it has been shown that injected BMDMs migrate towards the lesion site in response to the presence of chemokines associated with neuroinflammation (47).

5.2. Targeting cathepsin D to improve the functional recovery after SCI

The goal of this project was to analyse the catD protein expression pattern at different time points after inducing SCI. Secondly, we intended to gain knowledge about the potential of catD inhibitors to improve the functional recovery. Initially, significantly increased levels of intermediate catD were observed at day 4 post-injury. This was associated with elevated levels of mature catD from day 4 until day 10 post-injury. These data suggested that from day 1 until day 4 post-injury, there is an upregulated catD synthesis in the ER of neurons, astrocytes and macrophages, resulting in elevated levels of intermediate catD at day 4 post-injury. Moreover, this intermediate catD is rapidly cleaved, resulting in the formation of mature catD which resides at the lesion site from day 4 until day 10 post-injury. These results were in accordance with those published by Moon *et al.* They showed that at day 4 and 7 post-injury, the catD levels were significantly higher in the spinal cord of rats with a clip compression, compared to normal controls. Furthermore, they revealed that on day 4 post-injury, catD was profoundly detected in $CD68^{+}$- cells at the lesion site. Therefore, they suggested that catD could play a role in the phagocytotic and lysosomal activation of macrophages/microglia during SCI (29). Also in other inflammatory diseases such as chronic obstructive pulmonary disease and inflammatory bowel disease, an increased catD expression was observed in activated macrophages (52, 53). For these reasons, it could be that catD indirectly contributes to the neuroinflammatory response during different CNS disorders. However, it still remains unclear whether increased catD expression levels in macrophages are the cause or consequence of macrophages/microglial activation.

Since many studies have revealed that increased intra- and extracellular catD levels can induce neurotoxicity and stimulate detrimental inflammatory responses, we investigated the relevance of catD inhibitors to improve the functional recovery in SCI mice. The first catD inhibitor that we tested during this study was pep-A which is able to form a complex with catD, resulting in an impaired catD

enzymatic activity (30). Subsequently, it has been shown in neurons that pep-A reduced the proteolytic cleavage effects of catD and thereby decreased the cytosolic cytochrome c levels (32). Eventually, this attenuated the activation of caspase-mediated pathways, sparing neurons from toxic intracellular catD. Nevertheless, no improvements were observed in functional recovery of pep-A-treated mice, compared to control mice. Although these results were unexpected, they could be explained by the inability of pep-A to reduce neurotoxicity mediated by extracellular catD. Recently, Armitraj *et al.* indicated that toxic effects of extracellular catD were not dependent on its enzymatic activity, in contrast to intracellular catD, and could therefore not be inhibited by pep-A (32). Despite the fact that catD is normally targeted to the intracellular vesicles, it occurs that catD is also present in the extracellular environment. This is because in some CNS diseases and conditions, catD evades normal lysosomal packaging routes resulting in the secretion of catD in the environment. Although it remains speculative, neurotoxic effects of extracellular catD are associated with an impaired autophagy flux (32). This results in an uncontrolled autophagosome accumulation which can induce ER stress-induced apoptosis. This pathway can be blocked by 3-MA, which is a selective inhibitor of LC3-II, an important component of the autophagosome membrane. Subsequently, 3-MA can decrease the formation of autophagosomes (54).

Consequently, in a second *in vivo* experiment, both intra-and extracellular neurotoxic pathways of catD were blocked by injecting pep-A in combination with 3-MA in SCI mice. However, total blocking of catD revealed no significant differences in the functional recovery between the experimental and control group. Taken together, these data suggested that blocking catD has no significant effects on the functional recovery after SCI.

5.3. The effects of plant sterols on the regenerative process after SCI

Recent studies revealed that dietary PS profoundly accumulate inside the CNS (55). These findings have led to an increased interest in the physiological role of PS during different CNS disorders. The goal for this project was to reveal the potential therapeutic effects of PS in improving the functional recovery after SCI. It has been shown that Abcg5$^{-/-}$ mice displayed up to 12-fold upregulated PS levels in their circulation compared the WT mice (56). During a first *in vivo* experiment, the functional recovery of Abcg5$^{-/-}$ mice was compared to that of WT mice. Although the functional recovery in Abcg5$^{-/-}$ mice was aggravated compared to WT mice, the observed differences did not reach statistical significance. However due to insufficient backcrossing of Abcg5$^{-/-}$ mice into the C57Bl/6 background (which is the background of the control group), no conclusions can be set about the observed difference in the BMS score as they might be caused by genetic differences. Accordingly, the importance of the genetic

background when doing KO studies was stressed in a paper by Geurts *et al.,* were an increased susceptibility for a malaria infection was observed in mice bearing a TLR9 null mutation compared to WT mice. However, this was triggered by the heterogeneous genetic background of the mice instead of the TLR9 gene itself (57). Therefore, when working with genetically modified mice, it is of upmost importance to control the genetic background of both mutant and WT mice.

In a second *in vivo* experiment, were the experimental mice group was fed with a PS-enriched diet, no significant differences were observed in the functional recovery between the experimental and control group. This was an unexpected result since many articles highlight the beneficial anti-inflammatory and neuroprotective effects of PS in the CNS, resulting in an improved prognosis (35). For instance, Valerio *et al.* reported that a daily administration of PS suppressed the inflammatory-mediated CNS demyelination, resulting in a decreased disease severity in EAE, a mouse model of multiple sclerosis (58). However, the reason why PS have beneficial effects in some pathologies, while having non or even detrimental effects in other diseases remains to be elucidated. Yet, other studies also revealed a potential neurotoxic role for PS, mediated by glutamate excitotoxicity and their stimulatory effect on ROS production (59, 60). Moreover, it could be that depending on the specific disease pathology, the detrimental effects of PS are overwhelmed by its beneficial properties, while in other pathologies, the detrimental effects take the upper hand. Furthermore, it could also be that the effects of PS alone are not sufficient enough to induce improvements in the functional recovery in SCI mice.

6. Conclusion and future perspectives

The goal of this thesis project was to investigate different approaches that target both the pro-inflammatory and cytotoxic microenvironment to improve functional recovery after SCI. In a first part of the study, BMDMs were transduced with an IL-13 LV to create IL-13-overexpressing BMDMs. ELISA indicated that these transduced BMDMs secreted significantly upregulated levels of IL-13 compared to control groups. Moreover, we showed that IL-13 BMDMs are able to create an IL-13-enriched environment, polarizing themselves and other naïve macrophages towards an M2 phenotype *in vitro*. These data suggest that adoptive transfer of IL-13 BMDMs in SCI mice can result in a sustained IL-13 production at the lesion site which may prevent endogenous and tissue resident macrophages from polarizing towards a detrimental M1 phenotype.

In a second part of the study, we investigated the potential of catD inhibitors to improve the functional recovery after SCI. Significantly increased levels of intermediate catD were observed at day 4 post-injury. Subsequently, elevated levels of mature catD were detected from day 4 until day 10 post-injury. Moreover, we have shown that the catD inhibitors pep-A and 3-MA did not affect the functional recovery in SCI mice. Furthermore, we have also studied the potential therapeutic effects of PS to improve the functional recovery after SCI. However, our data provide evidence that PS do not improve the functional recovery after SCI.

Taken together, we can conclude that PS or catD inhibitors (pep-A and 3-mA) are not sufficient enough to overcome the growth-inhibitory environment created after SCI. Furthermore, IL-13 BMDMs can create an IL-13-enriched environment, polarizing macrophages towards an M2 phenotype. To investigate the effect of IL-13 BMDMs on the functional recovery in SCI mice, further *in vivo* studies are required were IL-13 BMDMs are injected in SCI mice. Moreover, after adoptive transfer of labeled IL-13 BMDMs *in vivo*, it could be interesting to perform immunohistochemical stainings on the spinal cord of SCI mice to investigate the migration and homing abilities of IL-13 BMDMs *in vivo*. Eventually, these future experiments will reveal the potential of IL-13 BMDMs as a therapeutic strategy to promote tissue repair and to improve the functional recovery after SCI.

References

1. DePaul MA, Palmer M, Lang BT, Cutrone R, Tran AP, Madalena KM, et al. Intravenous multipotent adult progenitor cell treatment decreases inflammation leading to functional recovery following spinal cord injury. Sci Rep. 2015;5:16795.

2. Silva NA, Sousa N, Reis RL, Salgado AJ. From basics to clinical: a comprehensive review on spinal cord injury. Prog Neurobiol. 2014;114:25-57.

3. Varma AK, Das A, Wallace G, Barry J, Vertegel AA, Ray SK, et al. Spinal cord injury: a review of current therapy, future treatments, and basic science frontiers. Neurochem Res. 2013;38(5):895-905.

4. Thuret S, Moon LD, Gage FH. Therapeutic interventions after spinal cord injury. Nature reviews Neuroscience. 2006;7(8):628-43.

5. Oyinbo CA. Secondary injury mechanisms in traumatic spinal cord injury: a nugget of this multiply cascade. Acta Neurobiol Exp (Wars). 2011;71(2):281-99.

6. Teng YD, Lavik EB, Qu X, Park KI, Ourednik J, Zurakowski D, et al. Functional recovery following traumatic spinal cord injury mediated by a unique polymer scaffold seeded with neural stem cells. Proc Natl Acad Sci U S A. 2002;99(5):3024-9.

7. Silver J, Miller JH. Regeneration beyond the glial scar. Nat Rev Neurosci. 2004;5(2):146-56.

8. Yiu G, He Z. Glial inhibition of CNS axon regeneration. Nat Rev Neurosci. 2006;7(8):617-27.

9. Ren Y, Young W. Managing inflammation after spinal cord injury through manipulation of macrophage function. Neural Plast. 2013;2013:945034.

10. David S, Kroner A. Repertoire of microglial and macrophage responses after spinal cord injury. Nat Rev Neurosci. 2011;12(7):388-99.

11. Zhou X, He X, Ren Y. Function of microglia and macrophages in secondary damage after spinal cord injury. Neural Regen Res. 2014;9(20):1787-95.

12. Ma SF, Chen YJ, Zhang JX, Shen L, Wang R, Zhou JS, et al. Adoptive transfer of M2 macrophages promotes locomotor recovery in adult rats after spinal cord injury. Brain Behav Immun. 2015;45:157-70.

13. Kigerl KA, Gensel JC, Ankeny DP, Alexander JK, Donnelly DJ, Popovich PG. Identification of two distinct macrophage subsets with divergent effects causing either neurotoxicity or regeneration in the injured mouse spinal cord. J Neurosci. 2009;29(43):13435-44.

14. Koyasu S, Moro K. Th2-type innate immune responses mediated by natural helper cells. Ann N Y Acad Sci. 2013;1283:43-9.

15. Hershey GK. IL-13 receptors and signaling pathways: an evolving web. J Allergy Clin Immunol. 2003;111(4):677-90; quiz 91.

16. Vidal PM, Lemmens E, Dooley D, Hendrix S. The role of "anti-inflammatory" cytokines in axon regeneration. Cytokine Growth Factor Rev. 2013;24(1):1-12.

17. Doherty TM, Kastelein R, Menon S, Andrade S, Coffman RL. Modulation of murine macrophage function by IL-13. J Immunol. 1993;151(12):7151-60.

18. Nakajima H, Uchida K, Guerrero AR, Watanabe S, Sugita D, Takeura N, et al. Transplantation of mesenchymal stem cells promotes an alternative pathway of macrophage activation and functional recovery after spinal cord injury. Journal of neurotrauma. 2012;29(8):1614-25.

19. Sindrilaru A, Scharffetter-Kochanek K. Disclosure of the Culprits: Macrophages-Versatile Regulators of Wound Healing. Adv Wound Care (New Rochelle). 2013;2(7):357-68.

20. Shin T, Ahn M, Moon C, Kim S, Sim KB. Alternatively activated macrophages in spinal cord injury and remission: another mechanism for repair? Mol Neurobiol. 2013;47(3):1011-9.

21. Gordon S. Alternative activation of macrophages. Nat Rev Immunol. 2003;3(1):23-35.

22. Dooley D, EL, TV, SL, NDV, DLB, et al. Mesenchymal stem cells overexpressing IL-13 decrease lesion size and demyelination after spinal cord injury. journal of neuroimmunology; 2014.

23. Yao A, Liu F, Chen K, Tang L, Liu L, Zhang K, et al. Programmed death 1 deficiency induces the polarization of macrophages/microglia to the M1 phenotype after spinal cord injury in mice. Neurotherapeutics. 2014;11(3):636-50.

24. Lee J, Ryu H, Ferrante RJ, Morris SM, Ratan RR. Translational control of inducible nitric oxide synthase expression by arginine can explain the arginine paradox. Proc Natl Acad Sci U S A. 2003;100(8):4843-8.

25. Estévez AG, Sahawneh MA, Lange PS, Bae N, Egea M, Ratan RR. Arginase 1 regulation of nitric oxide production is key to survival of trophic factor-deprived motor neurons. J Neurosci. 2006;26(33):8512-6.

26. Maruyama W, Kato Y, Yamamoto T, Oh-Hashi K, Hashizume Y, Naoi M. Peroxynitrite induces neuronal cell death in aging and age-associated disorders: A review. J Am Aging Assoc. 2001;24(1):11-8.

27. Briken V, Mosser DM. Editorial: switching on arginase in M2 macrophages. Journal of leukocyte biology. 2011;90(5):839-41.

28. Cai D, Deng K, Mellado W, Lee J, Ratan RR, Filbin MT. Arginase I and polyamines act downstream from cyclic AMP in overcoming inhibition of axonal growth MAG and myelin in vitro. Neuron. 2002;35(4):711-9.

29. Moon C, Lee TK, Kim H, Ahn M, Lee Y, Kim MD, et al. Immunohistochemical study of cathepsin D in the spinal cords of rats with clip compression injury. The Journal of veterinary medical science / the Japanese Society of Veterinary Science. 2008;70(9):937-41.

30. Benes P, Vetvicka V, Fusek M. Cathepsin D--many functions of one aspartic protease. Crit Rev Oncol Hematol. 2008;68(1):12-28.

31. Hashimoto M, Koda M, Ino H, Yoshinaga K, Murata A, Yamazaki M, et al. Gene expression profiling of cathepsin D, metallothioneins-1 and -2, osteopontin, and tenascin-C in a mouse spinal cord injury model by cDNA microarray analysis. Acta neuropathologica. 2005;109(2):165-80.

32. Amritraj A, Wang Y, Revett TJ, Vergote D, Westaway D, Kar S. Role of cathepsin D in U18666A-induced neuronal cell death: potential implication in Niemann-Pick type C disease pathogenesis. The Journal of biological chemistry. 2013;288(5):3136-52.

33. Kim S, Ock J, Kim AK, Lee HW, Cho JY, Kim DR, et al. Neurotoxicity of microglial cathepsin D revealed by secretome analysis. J Neurochem. 2007;103(6):2640-50.

34. Liu S, Sarkar C, Dinizo M, Faden AI, Koh EY, Lipinski MM, et al. Disrupted autophagy after spinal cord injury is associated with ER stress and neuronal cell death. Cell death & disease. 2015;6:e1582.

35. Vanmierlo T, Bogie JF, Mailleux J, Vanmol J, Lütjohann D, Mulder M, et al. Plant sterols: Friend or foe in CNS disorders? Prog Lipid Res. 2015;58:26-39.

36. Saeed AA, Genové G, Li T, Lütjohann D, Olin M, Mast N, et al. Effects of a disrupted blood-brain barrier on cholesterol homeostasis in the brain. J Biol Chem. 2014;289(34):23712-22.

37. Lech M, Anders HJ. Macrophages and fibrosis: How resident and infiltrating mononuclear phagocytes orchestrate all phases of tissue injury and repair. Biochim Biophys Acta. 2013;1832(7):989-97.

38. Tiscornia G, Singer O, Verma IM. Production and purification of lentiviral vectors. Nat Protoc. 2006;1(1):241-5.

39. Nelissen S, Vangansewinkel T, Geurts N, Geboes L, Lemmens E, Vidal PM, et al. Mast cells protect from post-traumatic spinal cord damage in mice by degrading inflammation-associated cytokines via mouse mast cell protease 4. Neurobiology of disease. 2014;62:260-72.

40. Basso DM, Fisher LC, Anderson AJ, Jakeman LB, McTigue DM, Popovich PG. Basso Mouse Scale for locomotion detects differences in recovery after spinal cord injury in five common mouse strains. Journal of neurotrauma. 2006;23(5):635-59.

41. Ishii H, Jin X, Ueno M, Tanabe S, Kubo T, Serada S, et al. Adoptive transfer of Th1-conditioned lymphocytes promotes axonal remodeling and functional recovery after spinal cord injury. Cell Death Dis. 2012;3:e363.

42. Hu JG, Shen L, Wang R, Wang QY, Zhang C, Xi J, et al. Effects of Olig2-overexpressing neural stem cells and myelin basic protein-activated T cells on recovery from spinal cord injury. Neurotherapeutics. 2012;9(2):422-45.

43. Schwartz M, Yoles E. Immune-based therapy for spinal cord repair: autologous macrophages and beyond. J Neurotrauma. 2006;23(3-4):360-70.

44. Zeng L, Yang S, Wu C, Ye L, Lu Y. Effective transduction of primary mouse blood- and bone marrow-derived monocytes/macrophages by HIV-based defective lentiviral vectors. J Virol Methods. 2006;134(1-2):66-73.

45. Hoornaert CJ, Luyckx E, Reekmans K, Dhainaut M, Guglielmetti C, Le Blon D, et al. In Vivo Interleukin-13-Primed Macrophages Contribute to Reduced Alloantigen-Specific T Cell Activation and Prolong Immunological Survival of Allogeneic Mesenchymal Stem Cell Implants. Stem Cells. 2016.

46. Herberts CA, Kwa MS, Hermsen HP. Risk factors in the development of stem cell therapy. J Transl Med. 2011;9:29.

47. Vogel DY, Heijnen PD, Breur M, de Vries HE, Tool AT, Amor S, et al. Macrophages migrate in an activation-dependent manner to chemokines involved in neuroinflammation. J Neuroinflammation. 2014;11:23.

48. Kroner A, Greenhalgh AD, Zarruk JG, Passos Dos Santos R, Gaestel M, David S. TNF and increased intracellular iron alter macrophage polarization to a detrimental M1 phenotype in the injured spinal cord. Neuron. 2014;83(5):1098-116.

49. Walthers CM, Seidlits SK. Gene delivery strategies to promote spinal cord repair. Biomark Insights. 2015;10(Suppl 1):11-29.

50. Boehler RM, Kuo R, Shin S, Goodman AG, Pilecki MA, Gower RM, et al. Lentivirus delivery of IL-10 to promote and sustain macrophage polarization towards an anti-inflammatory phenotype. Biotechnol Bioeng. 2014;111(6):1210-21.

51. Zhang X, Edwards JP, Mosser DM. The expression of exogenous genes in macrophages: obstacles and opportunities. Methods Mol Biol. 2009;531:123-43.

52. Bracke K, Cataldo D, Maes T, Gueders M, Noël A, Foidart JM, et al. Matrix metalloproteinase-12 and cathepsin D expression in pulmonary macrophages and dendritic cells of cigarette smoke-exposed mice. Int Arch Allergy Immunol. 2005;138(2):169-79.

53. Hausmann M, Obermeier F, Schreiter K, Spottl T, Falk W, Schölmerich J, et al. Cathepsin D is up-regulated in inflammatory bowel disease macrophages. Clin Exp Immunol. 2004;136(1):157-67.

54. Rideout HJ, Lang-Rollin I, Stefanis L. Involvement of macroautophagy in the dissolution of neuronal inclusions. Int J Biochem Cell Biol. 2004;36(12):2551-62.

55. Vanmierlo T, Weingärtner O, van der Pol S, Husche C, Kerksiek A, Friedrichs S, et al. Dietary intake of plant sterols stably increases plant sterol levels in the murine brain. J Lipid Res. 2012;53(4):726-35.

56. Jansen PJ, Lütjohann D, Abildayeva K, Vanmierlo T, Plösch T, Plat J, et al. Dietary plant sterols accumulate in the brain. Biochim Biophys Acta. 2006;1761(4):445-53.

57. Geurts N, Martens E, Verhenne S, Lays N, Thijs G, Magez S, et al. Insufficiently defined genetic background confounds phenotypes in transgenic studies as exemplified by malaria infection in Tlr9 knockout mice. PLoS One. 2011;6(11):e27131.

58. Valerio M, Liu HB, Heffner R, Zivadinov R, Ramanathan M, Weinstock-Guttman B, et al. Phytosterols ameliorate clinical manifestations and inflammation in experimental autoimmune encephalomyelitis. Inflamm Res. 2011;60(5):457-65.

59. Panov A, Kubalik N, Brooks BR, Shaw CA. In vitro effects of cholesterol β-D-glucoside, cholesterol and cycad phytosterol glucosides on respiration and reactive oxygen species generation in brain mitochondria. J Membr Biol. 2010;237(2-3):71-7.

60. Tabata RC, Wilson JM, Ly P, Zwiegers P, Kwok D, Van Kampen JM, et al. Chronic exposure to dietary sterol glucosides is neurotoxic to motor neurons and induces an ALS-PDC phenotype. Neuromolecular Med. 2008;10(1):24-39.

Auteursrechtelijke overeenkomst

Ik/wij verlenen het wereldwijde auteursrecht voor de ingediende eindverhandeling:
Targeting the pro-inflammatory and cytotoxic environment to improve functional recovery after SCI

Richting: **master in de biomedische wetenschappen-klinische moleculaire wetenschappen**
Jaar: **2016**

in alle mogelijke mediaformaten, - bestaande en in de toekomst te ontwikkelen - , aan de Universiteit Hasselt.

Niet tegenstaand deze toekenning van het auteursrecht aan de Universiteit Hasselt behoud ik als auteur het recht om de eindverhandeling, - in zijn geheel of gedeeltelijk -, vrij te reproduceren, (her)publiceren of distribueren zonder de toelating te moeten verkrijgen van de Universiteit Hasselt.

Ik bevestig dat de eindverhandeling mijn origineel werk is, en dat ik het recht heb om de rechten te verlenen die in deze overeenkomst worden beschreven. Ik verklaar tevens dat de eindverhandeling, naar mijn weten, het auteursrecht van anderen niet overtreedt.

Ik verklaar tevens dat ik voor het materiaal in de eindverhandeling dat beschermd wordt door het auteursrecht, de nodige toelatingen heb verkregen zodat ik deze ook aan de Universiteit Hasselt kan overdragen en dat dit duidelijk in de tekst en inhoud van de eindverhandeling werd genotificeerd.

Universiteit Hasselt zal mij als auteur(s) van de eindverhandeling identificeren en zal geen wijzigingen aanbrengen aan de eindverhandeling, uitgezonderd deze toegelaten door deze overeenkomst.

Voor akkoord,

Jonckers, Joren

Datum: **8/06/2016**